THE SYSTEMATIC PROPERTIES OF CLUSTERS OF GALAXIES

Thesis by

Augustus Oemler, Jr.

In Partial Fulfillment of the Requirements

for the Degree of

Doctor of Philosophy

California Institute of Technology

Pasadena, California

1974

(Submitted December 13, 1973)

ACKNOWLEDGMENTS

This thesis owes very much to very many people, but I must especially thank:

Dr. James Gunn, my thesis advisor, for suggesting this project, for his guidance and for so much material and moral support as I struggled along;

Steven Shectman, Richard Gott and Paul Schechter for the hundreds of hours of talk which helped me decide how to do it and what it all meant;

Dr. S.J. Aarseth, for his great generosity in letting me use his unpublished models of clusters;

Dr. J.B. Oke, for his help in my battles with telescopes, machines and certain unmentionable organizations;

Gary Tuton, Ranny Adams, and, especially, Dennis Palm for their hospitality, even more than their assistance, on Palomar;

Larry Blakee and Martin Olsiewski for their help with the electronics.

To Mrs. Virginia Steele Scott I owe a very great debt for her generous support over the last two and one half years.

The National Science Foundation provided a graduate Traineeship for two years, and additional support under NSF grants GP-27304 and GP-28027.

And, finally, thank you to all of those friends, including

the above, who helped make Caltech a pleasant place in spite of Pasadena.

ABSTRACT

Fifteen rich clusters of galaxies have been studied on photoelectrically calibrated photographic plates. These plates were measured using new automatic photometry techniques. Data in the literature have been supplemented by new observations to obtain velocity dispersions in nine of these clusters.

Clusters can be divided by their galaxy content into three types: spiral rich, spiral poor, and those dominated by a cD galaxy. The luminosity functions of the latter two types are very similar, and differ significantly from that of galaxies in spiral rich clusters. The surface brightness profiles of the spiral poor and cD clusters agree in several respects with numerical models of collapsed clusters by Aarseth, but the spiral poor clusters are too irregular and have too little central concentration to be collapsed. All of the clusters have a local minimum in their profiles which cannot be explained.

Spiral rich clusters tend to be less dense than average and cD clusters more dense, but, in the mean, all clusters follow a constant density law independent of mass. The cD clusters and others with a high ratio of elliptical to spiral galaxies have mass to light ratios of about 225, while the mass to light ratio of spiral rich clusters is less than half

of this value. The collapse times calculated using these mass-luminosity ratios confirm that spiral rich clusters are still collapsing while the others are close to equilibrium. The degree of mass segregation in the collapsed clusters is close to that predicted by the Aarseth models and requires that most of the cluster mass be in the galaxies themselves rather than in a cluster-wide medium.

The decrease of the number of spirals towards the center of the collapsed clusters supports the idea that S0 galaxies are created by stripping the gas from spirals, and the spiral rich clusters can be expected to evolve into spiral poor clusters after collapse by this mechanism. The high proportion of elliptical galaxies in the cD clusters probably means that they are a distinct type of object, and not just a later evolutionary state of the spiral poor clusters.

TABLE OF CONTENTS

I.	INTRODUCTION	1
II.	OBSERVATIONS	
	a) Choice of Objects	2
	b) Photometric Observations	4
	c) Plate Measurement Methods	8
	d) Measurement of Clusters	13
III.	DATA ANALYSIS	
	a) Cluster Membership	23
	b) Total Magnitudes	26
	c) Data Reduction	28
	d) Numerical Models	42
IV.	CLUSTER VELOCITY DISPERSIONS	49
V.	ANALYSIS OF THE RESULTS	56
VI.	CONCLUSIONS	77
	REFERENCES	84

I. INTRODUCTION

Although there is considerable interest in clusters of galaxies, only a few have been studied in any detail. If we wish to obtain some understanding of the present characteristics and past evolution of clusters, we need information on a sufficiently large group of objects to permit separating their systematic properties from those that are accidental to a single cluster. In an attempt to provide some of these data, a study has been made of the luminosities, positions and morphological types of galaxies in fifteen clusters of widely varying form and richness. Also, sufficient galaxy redshifts have been obtained, from the literature and from new observations, to determine velocity dispersions in eight of these clusters. The significance of these observations has been evaluated with the help of unpublished numerical models of clusters calculated by Aarseth.

It was obvious that the only practical method to obtain such a large amount of data would be photometry of wide field photographic plates. This choice, in turn, necessitated the development of fast, automatic plate measurement methods. These methods will also be described below.

II. OBSERVATIONS

a) Choice of Objects

The objects to be studied were taken from Abell's (1958) catalogue of rich clusters. Within this catalogue, those objects were selected which, of each richness class, were the nearest examples not at excessively low galactic latitude, and not in fields confused by the presence of many other clusters. Except for its richness class, the characteristics of the cluster itself were not considered in making this choice.

Some of this group were not studied because of poor plate quality or the limitations of time. Also, two clusters were later added: A 2197 because of data in the literature on its internal velocity dispersion and ZwCl 1545.1 +2104 because it had already been studied for other reasons (Oemler, Gunn and Oke 1972). Therefore, while the original list was an unbiased sample, the final group of fifteen clusters is too small and too fortuitous a selection to permit conclusions about the frequencies of clusters with various characteristics within Abell's catalogue.

The final list is presented, along with the richness class, redshift and galactic latitude of each object, in the first four columns of Table 1. Unless otherwise noted,

TABLE 1

CLUSTERS STUDIED

Cluster	Richness	z	b	Emulsion
Abell 194	0	0.0181	-43°	IIIaJ
Abell 400	1	0.0231	-45°	103aF
Abell 539	1	0.0267	-17°	IIIaJ
Abell 665	5	0.183 *	+35°	IIIaJ
Abell 1228	1	0.0344	+70°	103aF
Abell 1314	0	0.0335	+64°	IIIaJ
Abell 1367	2	0.0205	+74°	IIIaJ
Abell 1413	3	0.1427	+77°	IIIaF
Coma cluster	2	0.0230	+87°	O98
Abell 1904	2	0.0719	+62°	103aF
Hercules cluster	2	0.0360	+44°	103aF
Abell 2197	1	0.0303	+43°	IIIaJ
Abell 2199	2	0.0312	+43°	103aF
Abell 2670	3	0.0753†	-69°	O98
Zw Cl 1545.1 +2104	1	0.263 §	+49°	O98

* Sargent (1973)

† Oemler (1973)

§ Oemler et al (1972)

the redshifts have been taken from Noonan (1973).

b) Photometric Observations

Green and red plates were obtained of each cluster, using either the Palomar 200-inch or 48-inch Schmidt telescope. All green exposures were made on baked IIIaJ plates behind a Wratten 4 filter. Red exposures on the 48-inch were made on 103aF, O98 and IIIaF emulsions and at the 200-inch on water-hypersensitized O98 emulsions, all behind 2.2 mm of Schott RG-1 filter. The 200-inch plates were taken by James Gunn and two of the 48-inch plates were taken by Steven Shectman. 200-inch plates were 5 x 7 inches in size, giving a usable field of 21'x 23'. 48-inch plates were either 5 x 7 in (2.0° x 2.1°), 10 x 10 in (4.3°x 4.3°) or 14 x 14 in (6.2°x 6.2°), depending on the angular extent of the cluster. All 10 x 10 in and 14 x 14 in plates had sensitometer spots placed on one corner and one plate from the same box was developed with each batch of 5 x 7 in plates. All plates were developed for nine minutes in MWP-2 developer, using a rocker agitator to ensure even development.

An attempt was made to expose all plates to a sky

density of about 0.5 in order to give reasonable densities in both the centers and outer envelopes of galaxies. However, because of variations in sky brightness and plate sensitivity, the actual sky densities vary rather widely. Because of serious emulsion defects which rendered them unsuitable for photometry, many plates could not be used. As a consequence of this, it was impossible to measure all clusters in one color. The emulsion of the plate that was used is presented, for each cluster, in the last column of Table 1. All plates were taken on the 48-inch telescope, except for those of A 2670, which came from both telescopes, and those of Zw Cl 1545.1 +2104.

Absolute calibration of these plates was obtained from photoelectric photometry of several galaxies in each field. Each galaxy was photometered through one large aperture, typically 40" in diameter for nearby objects. This was done with either the 200-inch multichannel spectrophotometer or a two-tube S20 photometer mounted on the Palomar 60-inch telescope. Filters for the 60-inch photometer were chosen to match as closely as possible the spectral response of the two photographic bands. Filters used were, in the green, 3mm Schott BG38, 1 mm Schott GG460 and a Wratten 44, and, in the red, 3 mm Schott RG1, 3 mm Schott BG20 and 1 mm Schott BG38.

The photographic and photoelectric response curves are presented in Figure 1. The green band, denoted by J, is

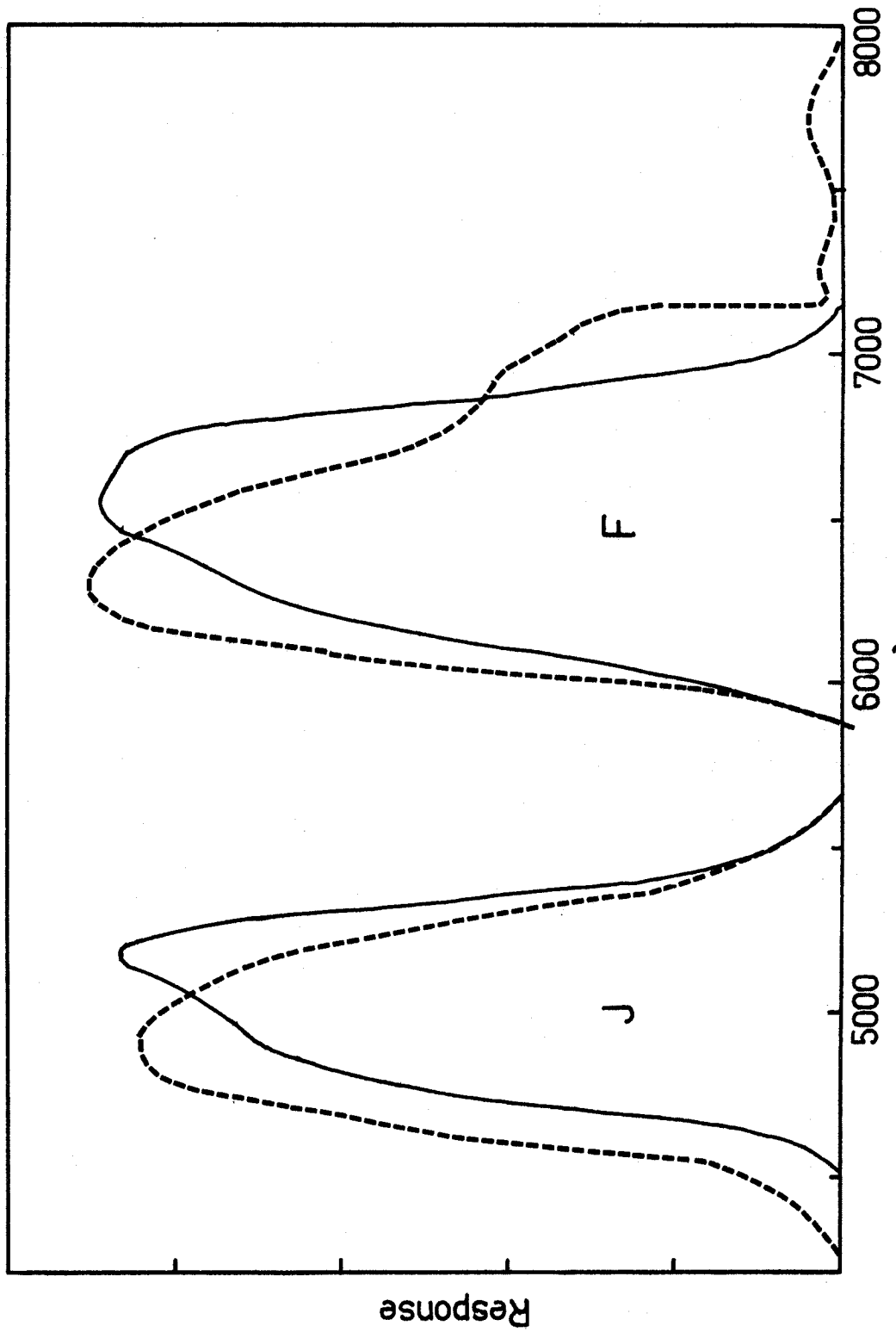

FIGURE 1.- Photoelectric (dashed curves) and photographic (solid curves) response functions for the J and F bands.

somewhat to the blue of the V band, and the red band, denoted by F, is similar to Sandage and Smith's (1963) R band, but is more sharply cut off at the red end. Magnitudes are defined so that, for an A0 star, J - F = 0.0 and J - V = 0.0 for the photographic bands. Both the 200-inch multichannel and 60-inch broadband photometry are tied to the absolute photometry of α Lyr (Oke and Schild 1970) through the multichannel spectrophotometer secondary standards. J and F magnitudes of standard stars and galaxies were constructed from the multichannel scans using the photographic response functions, but the differences between these and the photoelectric magnitudes of late spectral type objects are not significant for photometry of the accuracy used in this study. The photoelectric photometry showed that, for galaxies with late-type spectra, it is approximately true that

$$J = V + 0.35 \cdot (B-V) \qquad (1)$$

and

$$J - F = 1.1 \pm 0.10 \qquad (2)$$

There were no photoelectric data on one cluster, A 1413. Plates of this cluster were calibrated using Zwicky et al (1961) photometry of bright galaxies in the field. Comparison of Zwicky's photometry in other cluster fields with

that done for this study showed that, for $m_p < 15.0$, the magnitudes of late spectral type galaxies were related by

$$m_p = m_F + 1.5 \pm 0.2 \qquad (3)$$

c) Plate Measurement Methods

Two methods for the photometry of galaxies on photographic plates were used in this study. The first, which involves microphotometer tracings of galaxy images on a negative copy of the plate, has been described in detail elsewhere (Oemler 1973). This method was used on A 1314, A 539, A 2670 and Zw Cl 1545.1 +2104, but proved too time consuming for the very large amount of photometry which had to be done. The second method, a completely automated procedure for both finding and measuring galaxies, is based on the Caltech plate scanner. This machine is a two-axis microphotometer attached to a small computer. The computer controls carriage motion, processes the digitized output of the photometer and writes data on magnetic tape. Although of poor positional accuracy ($\sim$ 15 μ) and abysmal reliability, the photometer and optical system are of sufficient quality and dynamic range to measure the wide density range found on

deep photographic plates.

The galaxy measurement process is in two parts. In the first part, the area of the plate to be studied is scanned with a long, narrow slit in a raster pattern of 256 overlapping rows. On a large computer, the data along each row are added to form 1024 overlapping boxes per row. By overlapping in each direction, we ensure that no galaxy image will be missed because it fell half in one box and half in another. On even the best of plates, the sky background density varies over the field due to variations in plate sensitivity and fog. The variation in sky density is found by an iterative procedure of ignoring the denser than average points and fitting the remainder to a low order (3 to 5) two dimensional least squares polynomial fit.

Each star and galaxy in the measured field is represented by a group of points in the 256 x 1024 array of higher opacity than the least squares fit to the sky. All of those groups whose peak opacity differs from that of the sky by more than some threshold value are considered as objects to be photometered and their positions are added to a list on magnetic tape for the plate scanner. The peak opacity of each chosen point and the sky fit are saved for later use.

In the second part of the measurement process, the plate scanner moves in turn to each position on the list and

performs a raster scan of a small square area. The aperture size and digitizing rate are chosen so that each data point covers one resolution element on the plate. Since the coordinates provided by the search routine are rather crude, 1/256 x 1/1024 of the scanned area, the object is often not centered in the small area measured. Therefore, the plate scanner checks the position of the object within the data array and, if sufficiently off center, performs another, correctly positioned, raster scan. The exact position and the digitized scan are recorded on tape for later reduction.

Among the objects which have been photometered, there are, typically, four times as many stars as galaxies. To separate the two groups, we make use of the fact that the images of stars are of higher surface brightness than those of galaxies. In Figure 2, the log of the mean opacity is plotted against the log of the area for a sample of objects in the Coma cluster. Stars are denoted by filled circles and galaxies by open circles. There is a clear separation of the two groups down to about log A = 1.5. This is close to the selection limit for these objects, but, on photometry of fainter objects, one can usually separate the two groups down to a magnitude where it is becoming difficult to distinguish stars from galaxies by eye. Most of the filled circles of lower than average opacity correspond to cases of two or more fainter stars in the measured area. The efficacy of

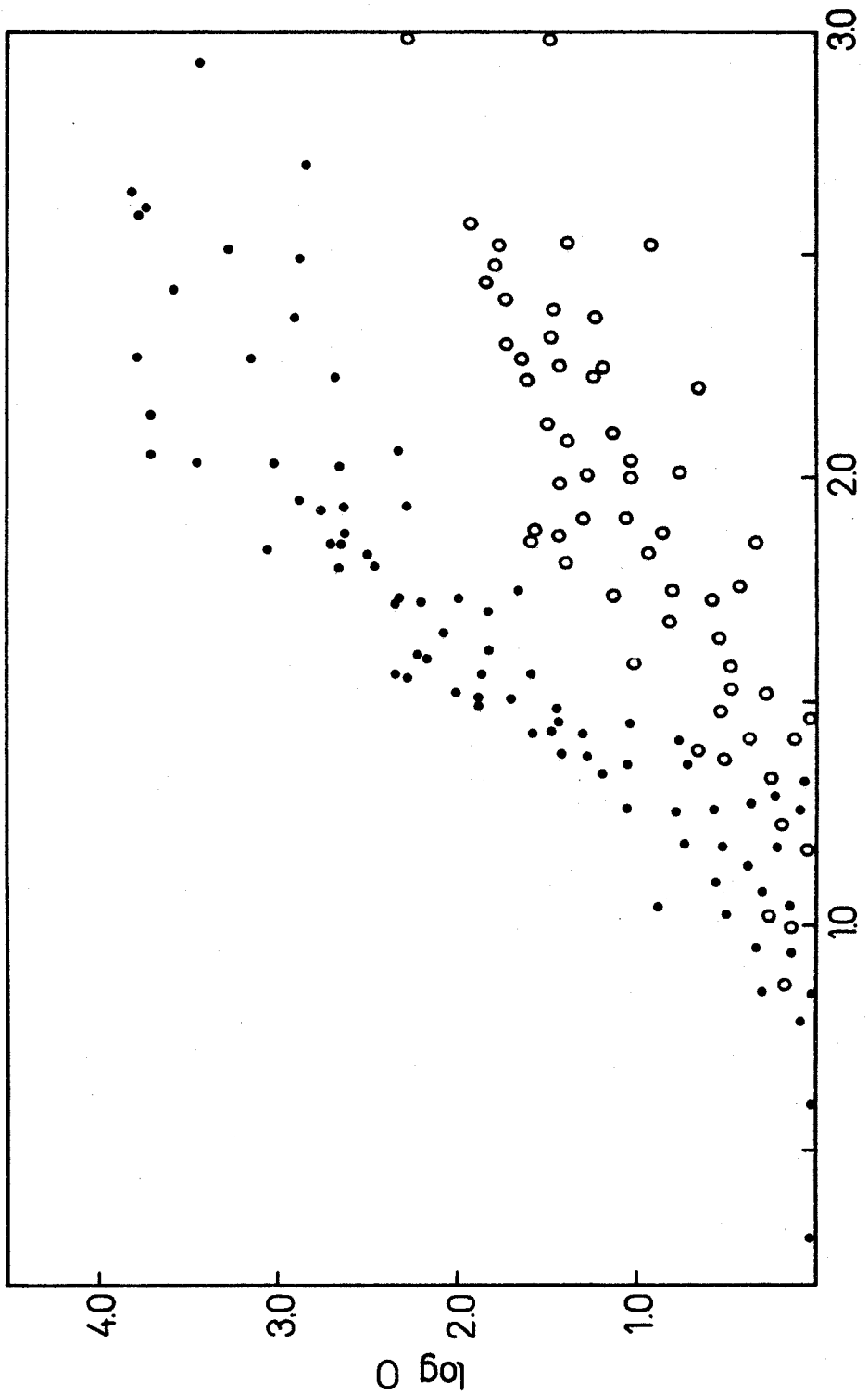

FIGURE 2.- Opacity versus area for a sample of stars (filled circles) and galaxies (open circles) in the Coma cluster.

the method may be improved at the expense of increased computing time, since much of the smearing of the star distribution is due to the crudity of the sky correction method used. In practice, the star rejection line is set slightly high so as not to miss any galaxies. A small number of objects near the line are inspected by eye to remove any stars.

Having eliminated all stars, obtaining the galaxy magnitudes is a straightforward procedure. All points in each raster scan are converted to relative surface brightnesses using the characteristic curve obtained from the sensitometer spots on each plate, then the sky background is removed using the least squares fit obtained earlier. The relative brightnesses are converted to absolute values using those galaxies for which we have photoelectric photometry. Now, to obtain the isophotal luminosity of an object, we simply add the intensities of all points whose surface brightnesses are greater than that of the limiting isophote.

The final step is to determine the limit of completeness of this group of objects. First the galaxies are divided into magnitude intervals. It will be recalled that the selection criterion for objects was the peak measured opacity of their images. For each magnitude interval, we plot a histogram of the number of objects of each peak opacity,

this quantity having been saved from the search routine. The result is a series of near-gaussian curves which, with increasing magnitude, are more and more truncated by the selection limit. Assuming the distributions to be symmetrical, we can calculate, for each case, the fraction of objects which fall below the threshold, and thus find the incompleteness as a function of magnitude.

This entire procedure for finding and measuring galaxies has several great virtues. One is that, by measuring all parts of the galaxy image, it has the potential of high accuracy. Another is that it is completely automatic, requiring intervention only to specify the criterion for separating stars from galaxies. Its practical efficiency and accuracy will be discussed below.

d) Measurement of Clusters

In studying a cluster, we wish to measure objects over as wide as possible a field and to as faint as possible a limiting magnitude. There are two considerations, one practical and one fundamental, which limit what can be done. The fundamental limit is set by the uncertain corrections for field objects, which increase rapidly in importance with field size and magnitude limit. This problem will be

considered in detail later. The number of objects which can be conveniently measured, given the limitations of time and data handling ability, provide the practical limit. In particular, since most objects found and measured are stars, evenly distributed over the field, increasing the area and the depth to which it is studied rapidly increases the measurement work. Typically, if we are limited to a few thousand objects per field, we can expect to measure no more than 500 galaxies.

Given these constraints, a compromise must be made in order to measure a sufficient area and a sufficient magnitude range of a cluster. First, a large field is measured over a restricted magnitude interval to survey the total extent of a cluster and obtain some measure of the galaxy background in its vicinity. Then, to obtain the faint end of the cluster luminosity function, a small field in the cluster center is measured to a much fainter limit.

A convenient measure of cluster scale is the Abell radius (Abell 1958) defined by

$$r_a = 5.15 \times 10^5 / cz \quad \text{arc min} \qquad (4)$$

If we assume, as we shall throughout this paper, a Hubble constant, H_o, of 50 km $s^{-1}Mpc^{-1}$ and a deceleration parameter, q_o, of 0.0, this is equivalent, for nearby objects,

to a linear size of 3.0 Mpc. For a typical cluster, about 80 percent of the total mass is contained within the Abell radius.

For most of the clusters in this study, photometry of galaxies in the brightest 3 magnitude interval has covered an area out to 2 or 3 Abell radii. Usually, faint galaxies within one Abell radius have been studied, although occasionally a somewhat smaller area was covered. The procedure of inferring the faint galaxy content of the entire cluster from a study of the center is legitimate only if there is no mass segregation due to two body relaxation. We shall show later that this is true, in the relevant mangitude range, for all clusters.

In measuring individual galaxies, the size of the raster scan was chosen to be large enough to contain the entire galaxy out to the desired limiting isophote, but not so large that there would be a significant chance of including another object in the measured area. Scan areas used varied from 2' square for the brighter galaxies in the nearest clusters to 10" square for the fainter galaxies in the most distant clusters. Normally, each data point covered a 2" square area, the resolution of good 48-inch telescope plates, but for some of the smaller scans a 1" area was used.

All galaxy photometry in this study was done to a limiting isophote of 24.1 mag per square second in the green

and, its equivalent, 23.0 mag per square second in the red. This proved to be the faintest surface brightness which could be used without encountering problems due to plate noise and incorrect subtraction of the sky brightness.

The accuracy of the two methods of photometry has been checked in several ways. Eight galaxies in each of the two clusters A 1228 and A 1367 were measured photoelectrically. When the galaxies, with a brightness range within each cluster of 2 mag, were used to calibrate plates of these clusters in the normal manner, the standard deviation in the calibration of individual objects was 0.11 mag, due to the combined errors in the photoelectric and in the photographic photometry. Results from the other 8 clusters with several calibration objects each gave a similar standard deviation of 0.10 mag.

Forty-eight objects were measured on each of two separately calibrated plates, one of very good and the other of rather poor quality, of the Coma cluster. There was no calibration difference. There was a systematic difference of 0.03 mag per magnitude in the magnitude scales, due probably to errors in the characteristic curves of the plates. The random differences between the two sets of measurements had a standard deviation of 0.13 mag, most of which can probably be attributed to the poor plate.

Twenty-seven objects were measured, with the plate scanner, on the plate of A 1314 which had previously been studied using the first photometry method. Any systematic difference in the magnitude scales was below the level of the random errors. This reassures us that there are no systematic errors in photometry with the plate scanner due to inaccurate measurements of the dense centers of galaxies, since the first photometry method uses a negative of the plate on which the galaxy centers are the least dense, most easily measured part. The random errors between the two sets of measurements had a standard deviation of 0.21 mag, which, assuming $\sigma = 0.09$ for the second method, implies $\sigma = 0.18$ for the first method.

The average reliability of photometry by the two methods can be summarized thus: for the first method, calibration errors $\sigma = 0.14$, random errors $\sigma = 0.18$; for the second method, calibration errors $\sigma = 0.07$, random errors $\sigma = 0.09$.

After photometry of each cluster was completed, a finding chart was prepared of all galaxies above the limit of completeness. The IIIaJ plate of the cluster was then inspected using this chart to see if any galaxies were missed or stars included in the final list of objects. In general, it was found that 1 to 2 percent of the galaxies in

the field brighter than the completeness limit had been missed for various reasons. A similar number of stars usually managed to slip through the screening processes. These omissions and inclusions were corrected.

For nearby clusters ($z \sim .04$), all of the galaxies in each field were classified by morphological type using the same IIIaJ plate. Objects were classified as ellipticals, SO's or spirals (including irregulars). Unfortunately, the classification of objects at distances of a few hundred megaparsecs on deep, small scale photographic plates is not very satisfactory. Necessarily, one is classifying the outer features of galaxies, while the usual morphological types are based on the nuclear properties of the galaxies, obtained from thin, large scale plates. Perhaps worse, the poor resolution obscures many features, making it especially difficult to distinguish SO and spiral galaxies. A comparison of classifications of objects in the Coma cluster and A194 with those of the same objects by Rood and Baum (1967) and Zwicky and Humason (1964) using 200-inch plates shows that, while E and S0 galaxies were typed fairly reliably, there was a systematic tendency to classify many early-type spirals as S0's.

Details of individual clusters are summarized below.

Abell 194 was studied by Zwicky and Humason (1964). It is a moderately regular cluster, in which the brightest

galaxies, most of which are S0's, form a long chain. The plate used was of only fair quality.

Abell 400 is a moderately regular cluster in which most of the bright galaxies are ellipticals and S0's. Only the inner part of the cluster was studied, necessitating large extrapolations in the later analysis. The plate studied was of only fair quality.

Abell 539 is similar in form and content to Abell 400. There is a short chain of bright galaxies in the center. This cluster is at low galactic latitude. There is much nearby obscuration, but the cluster itself does not seem to be obscured. A 5 x 7 in plate of good quality was studied to one limiting magnitude over the entire field.

Abell 665 is the only richness class 5 cluster in Abell's catalogue. Although there is some tendency to sub-clustering, there is no strong evidence that this is not one cluster. The plate studied was of fair quality.

Abell 1228 is an irregular cluster dominated by spiral galaxies. The plate studied was of good quality.

Abell 1314 is a regular cluster dominated by ellipticals. There is no one galaxy of outstanding brightness. The plate studied was of good quality.

Abell 1367 has a high spiral content but is fairly compact and regular in appearance, with several bright E's and S0's in the center. The plate used was of very good

quality.

Abell 1413 is a rich, regular cluster. The huge central cD galaxy was described by Morgan and Lesh (1965) as possibly the largest of all supergiant galaxies. The IIIaF plate used was deep but of poor quality.

The Coma cluster was studied on one 14 x 14 in plate of rather poor quality.

Abell 1904 is a rich, regular cluster with a central cD galaxy of moderate size. A good quality plate was photometered to a uniform depth over the entire field.

The Hercules cluster is an irregular cluster dominated by spiral galaxies. The small companion cluster Abell 2147 is located 2° to the South. A good quality plate was used.

Abell 2197 is a somewhat irregular cluster located 1.5° north of Abell 2199. The plate used was of good quality.

Abell 2199 is a compact, regular cluster. The large central galaxy, NGC 6166, is a type example of cD galaxies (Matthews, Morgan and Schmidt 1964.) A2197 and A2199 have the same redshift and a projected separation of only 4.5 Mpc. Assuming a velocity of approach of 1000 km s^{-1}, the collapse time of this system is only 4.5 billion years. However, there is no evidence that these two clusters are not, at present, independent systems. The distribution of galaxies in their vicinity brighter than $m_F = 15.0$ is presented in Figure 3. Each contour represents an increase

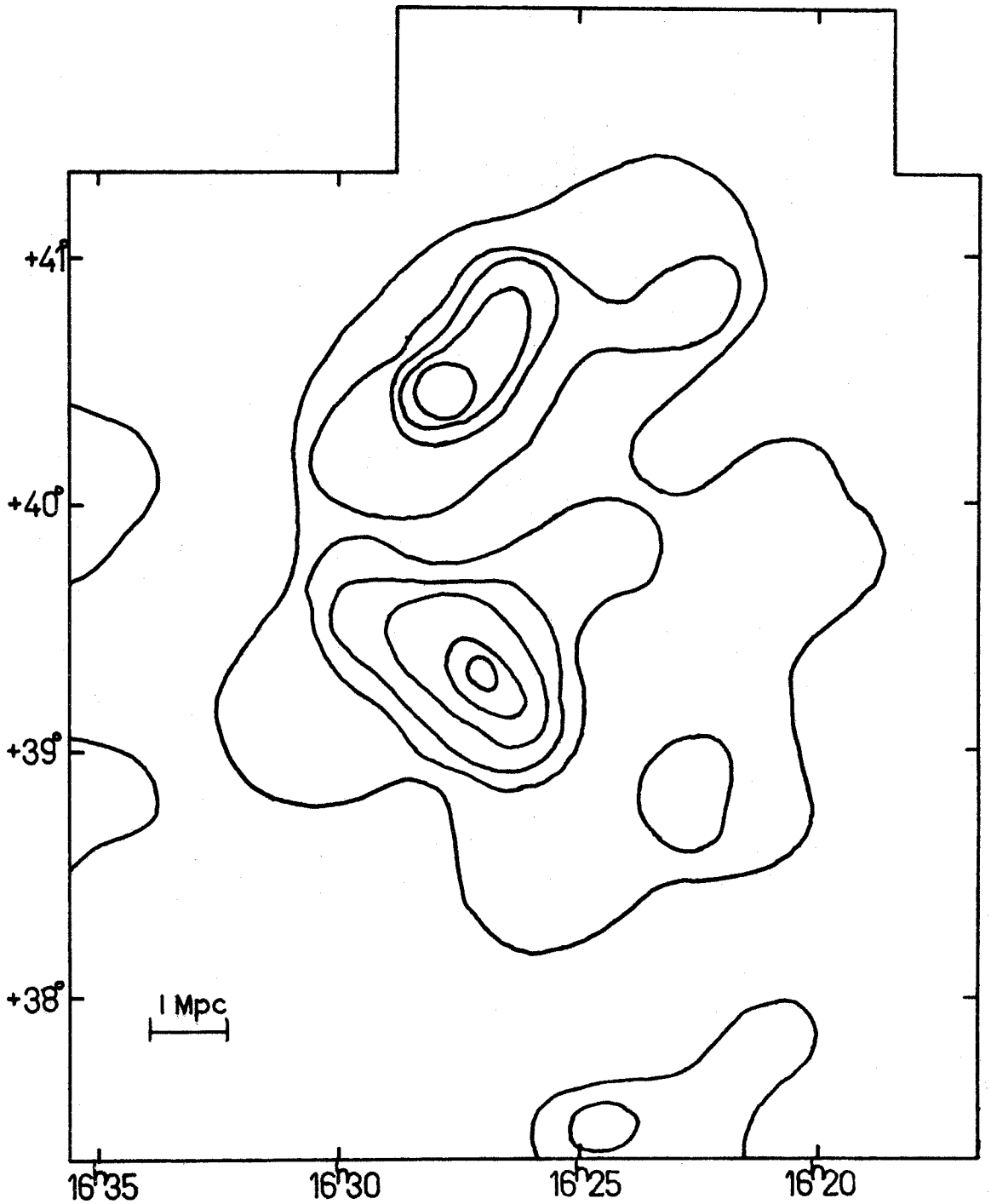

FIGURE 3.- The distribution of galaxies brighter than $m_F = 15.0$ in the area of A 2197 (top) and A 2199. The contour interval is 110 galaxies per square degree.

in surface density of 110 galaxies per square degree. Only the outermost contour overlaps and there appears to be no distortion of the inner contours due to interaction. Therefore, in the later analysis they will be treated as independent systems.

Abell 2670 is a compact, regular cluster with a central supergiant galaxy. It is discussed in detail in Oemler (1973.)

Zw Cl 1545.1 +2104 is similar in appearance, although not as rich, to A 2670. See Oemler et al (1972) for details.

III. DATA ANALYSIS

a) Cluster Membership

Much of the uncertainty, reflected in the literature, about the properties of clusters of galaxies is due to the difficulties of separating them from the general field of galaxies which surrounds them. Since many clusters are probably still undergoing collapse and/or infall, there are some problems with deciding which, even of the galaxies in their vicinity, should be considered cluster members. However, the most serious troubles are due to background galaxies. Fluctuations in the number density of background galaxies are strong on all scales, but particularly at those corresponding to the clustering scale of objects at a particular distance ($\sim$ apparent magnitude) (Shectman 1973,1974). These fluctuations, plus practical limitations on the area which can be studied, make it very difficult to accurately infer the contribution of background objects to a cluster of galaxies from counts in the vicinity of the cluster.

In order to make the most of the information available, all counts of field galaxies in each color have been combined into two mean distributions. It was found that, to the limits of accuracy set by the statistics, these two distributions could themselves be combined, with a color shift of

J-F = 0.90, into one number vs magnitude relation. All of the available data are presented in Figure 4. While most of the data come from the outer parts of cluster fields photometered for this study, they have been supplemented at the bright end with counts in a few fields by Zwicky et al (1961-1968) using the relation between the two photometric systems in equation 3. The dotted line in Figure 3 is the adopted mean relation used for all clusters. The scatter is quite large, not only from field to field, but also from point to point within one field. In all subsequent analysis, we will consider that the uncertainty in the background level is $\pm$ 50 percent.

It is obvious that this relation can be fit to the canonical log N = C+ 0.6.m law over only a limited magnitude range. The fall off at the faint end is expected due to the omitted k correction; however, the increase of number with magnitude of the bright galaxies does not seem to be consistent with a constant space density.

Among those galaxies bright enough to be classified by morphological type, there are 64 percent spirals, 23 percent S0's and 13 percent ellipticals. It will be assumed that these proportions are correct at all magnitudes.

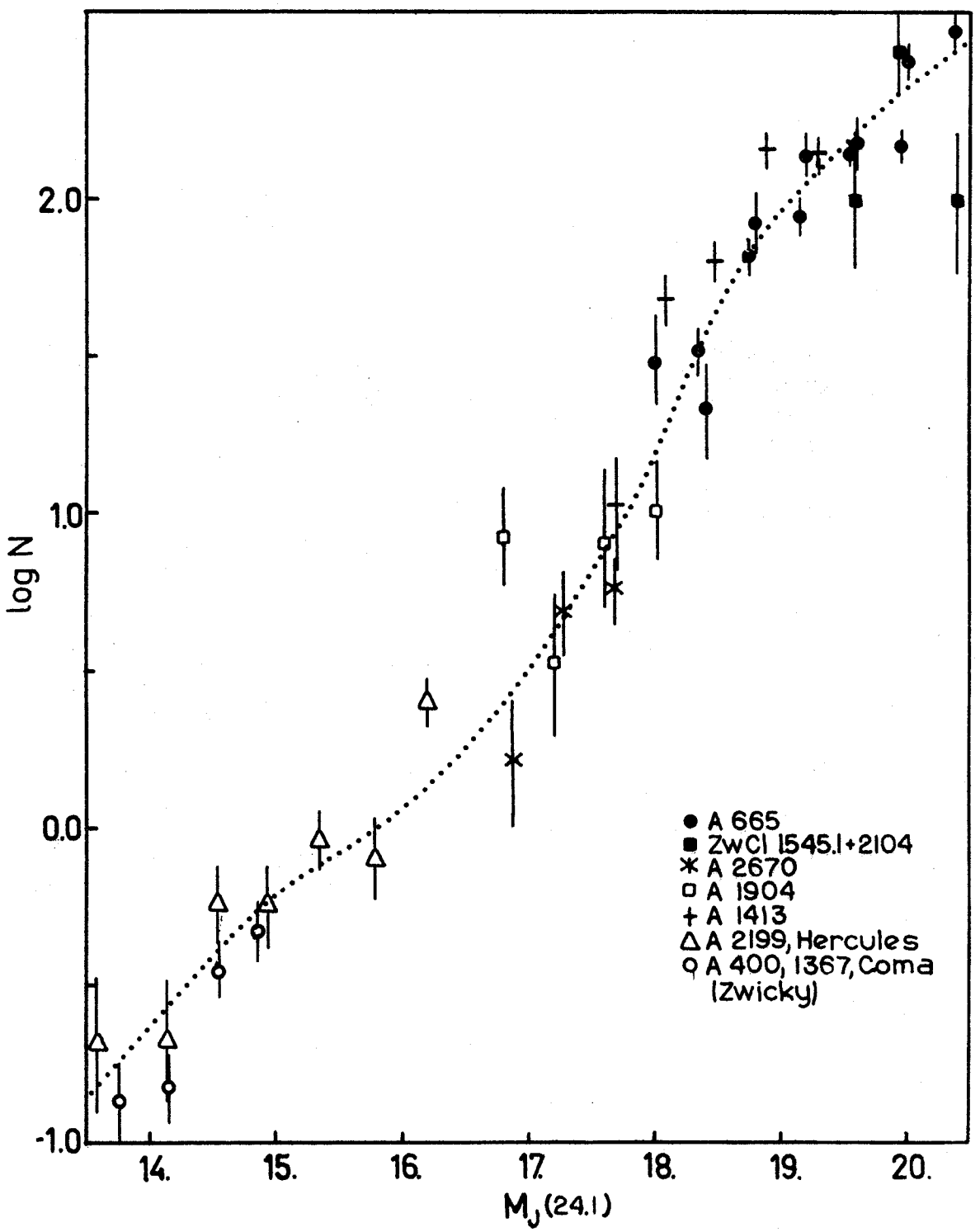

FIGURE 4.- The number density of field galaxies per 0.4 mag interval in fields near the indicated clusters of galaxies. The dotted line is the adopted relation for all fields.

b) Total Magnitudes

To find the total luminosity of a galaxy, one must extrapolate beyond the isophotal luminosity obtained from the photographic photometry. This procedure has been described in another paper (Oemler 1973) using a semiempirical analysis of the limited data available then. The reliability of the Coma cluster photometry (Rood and Baum 1968) on which that analysis heavily depended has recently been questioned by Ables and Ables (1972). The proper extrapolations have therefore been redetermined in a purely empirical manner, using raster scans of selected objects in the Coma cluster for which a very careful determination of the background level was made.

The results are presented in Figure 5, where spirals are denoted by x's, S0's by open circles and ellipticals by closed circles. As there appears to be no systematic difference with morphological type, the mean relation shown by the solid line will be used for all galaxies.

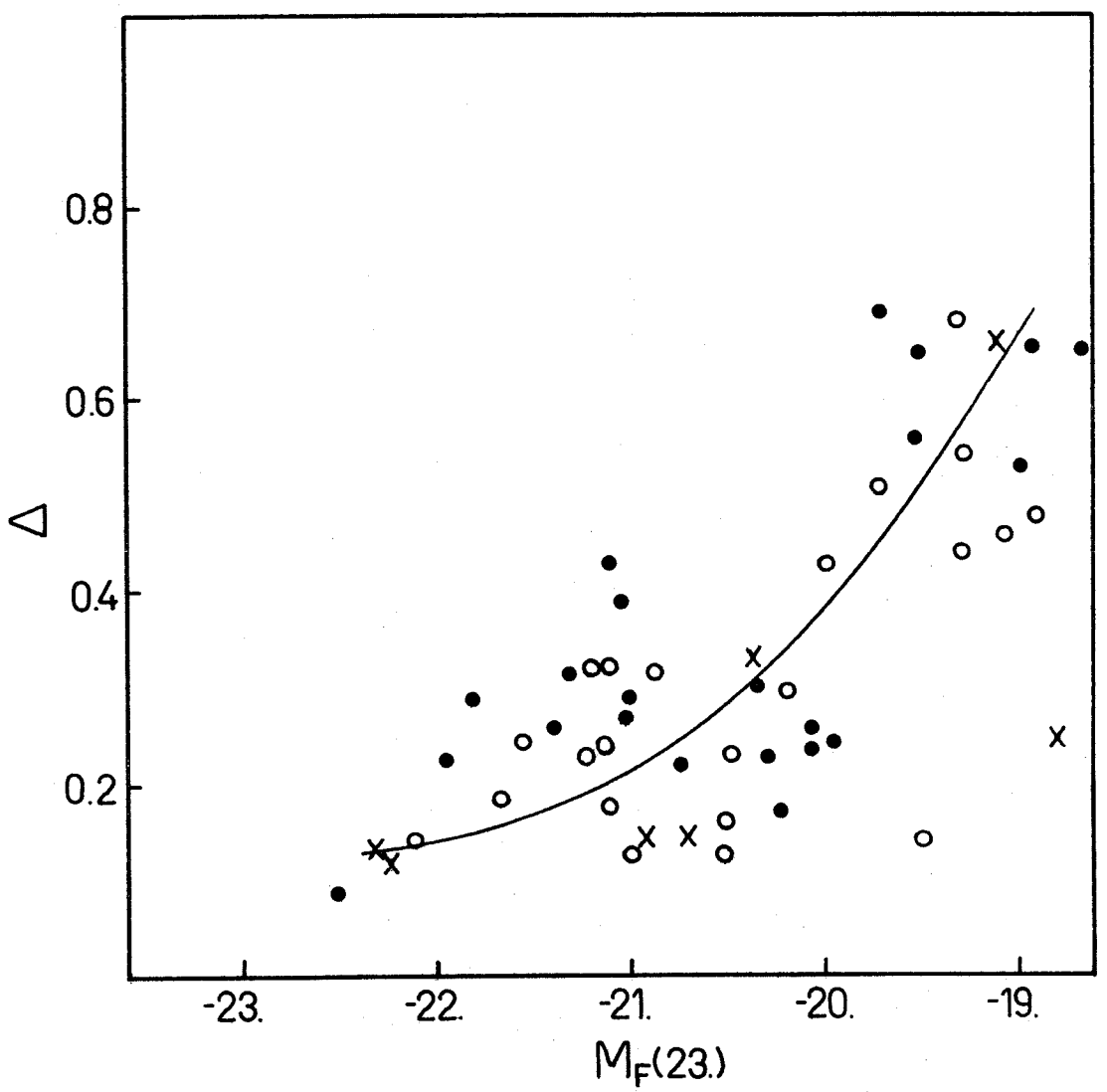

FIGURE 5.- Extrapolations from $m_F(23.)$ to total magnitudes for a sample of spirals (x's), S0's (open circles) and ellipticals (filled circles) in the Coma cluster.

c) Data Reduction

Using the background corrections determined above, luminosity functions were constructed for all clusters. Each luminosity function was extended to that magnitude where the incompleteness of the photometry reached 25 percent or where the contribution of the background to the galaxy counts reached one third. Before this point, the galaxy counts were corrected for the incompleteness at each magnitude calculated earlier. For those clusters which were studied in two fields of differing limiting magnitude, separate luminosity functions were constructed for each field. In the larger of the two fields, and in the single field when there was only one, the luminosity function was generally constructed from an area somewhat larger than that within one Abell radius. However, when improved signal to noise made it desirable, a larger or smaller area was used, so that the final luminosity functions cannot be used to directly obtain the cluster richness or total luminosity.

In the three cases, A2197, A 2199 and the Hercules cluster, where there was a neighboring cluster in the field, that quadrant of the field in the direction of the other cluster was omitted at radii greater than 30'. The luminosity function of the large field was extended to fainter magnitudes by renormalizing the luminosity function of the smaller

and deeper field so that the two agreed over the magnitude interval they had in common. In no case was there a statistically significant difference between the two curves.

The galaxy magnitudes were corrected for absorption within our own galaxy using the prescription given by Sandage (1973) which, for this photometric system, becomes

$$A_J = A_F = 0.0 \quad b > 50° \tag{5}$$

$$A_J = 0.11 \cdot (\csc b - 1) \quad b < 50° \tag{6}$$

$$A_F = 0.07 \cdot (\csc b - 1) \quad b < 50° \tag{7}$$

The only significant correction was that for A 539, where $A_J = 0.27$. Apparent isophotal magnitudes were converted to absolute isophotal magnitudes using the redshifts in Table 1. The k corrections were calculated for the more distant clusters using a scan of the central galaxy in A 2670 obtained by James Gunn. The redshift of Zw Cl 1545.1 +2104 is so great that the light observed in the F band was emitted at wavelengths close to the J band. Therefore, J rather than F magnitudes were calculated for this cluster. Luminosity functions for all clusters are presented in Figure 6. Open circles are galaxy counts per 0.4 mag interval and filled circles are integrated counts.

Spherical symmetry has been assumed in determining the cluster surface brightness profiles. This is not a very satisfactory approximation in some cases, such as A 194

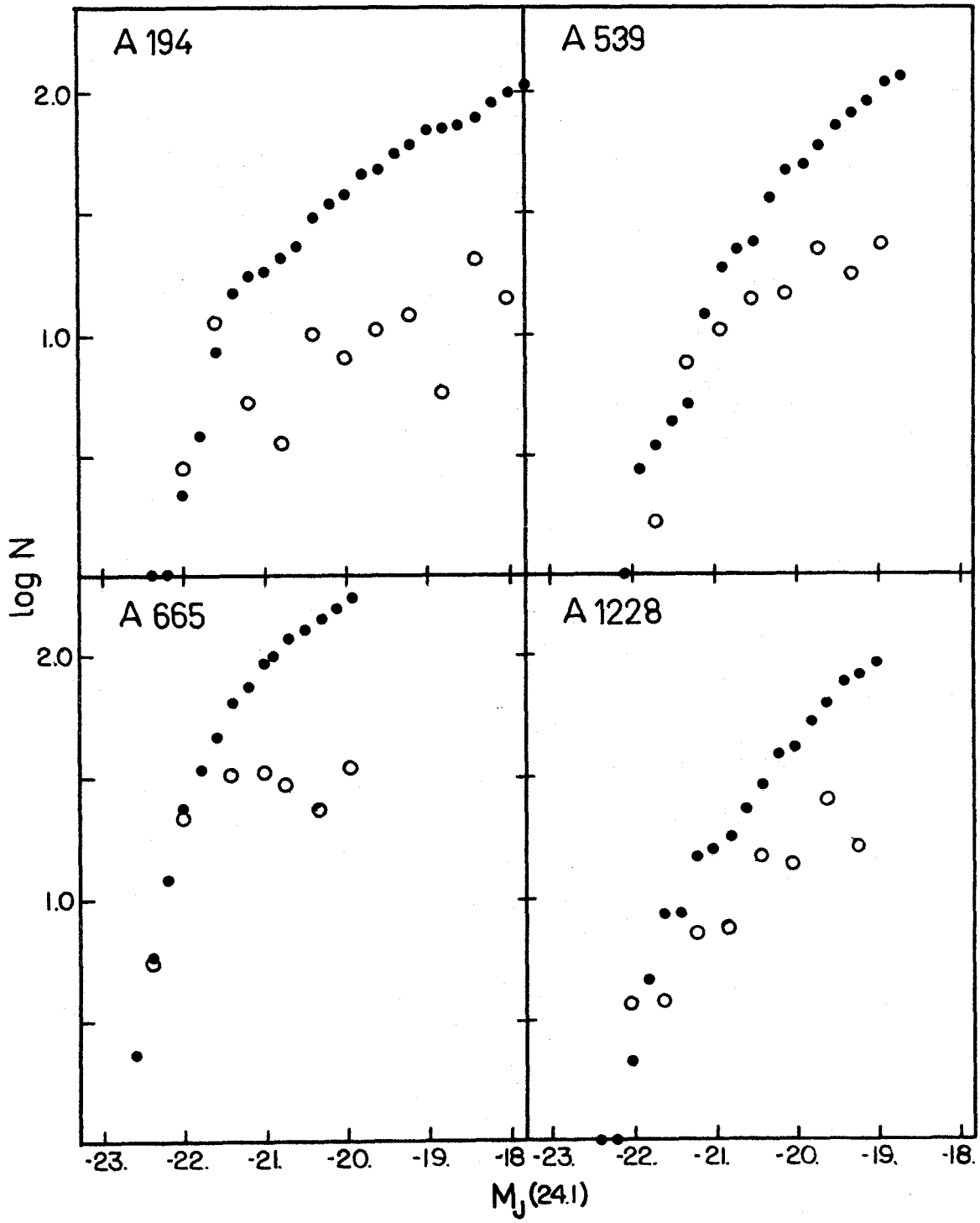

FIGURE 6.- The cluster luminosity functions. The open circles are galaxy counts per 0.4 mag interval, and the filled circles are integrated counts.

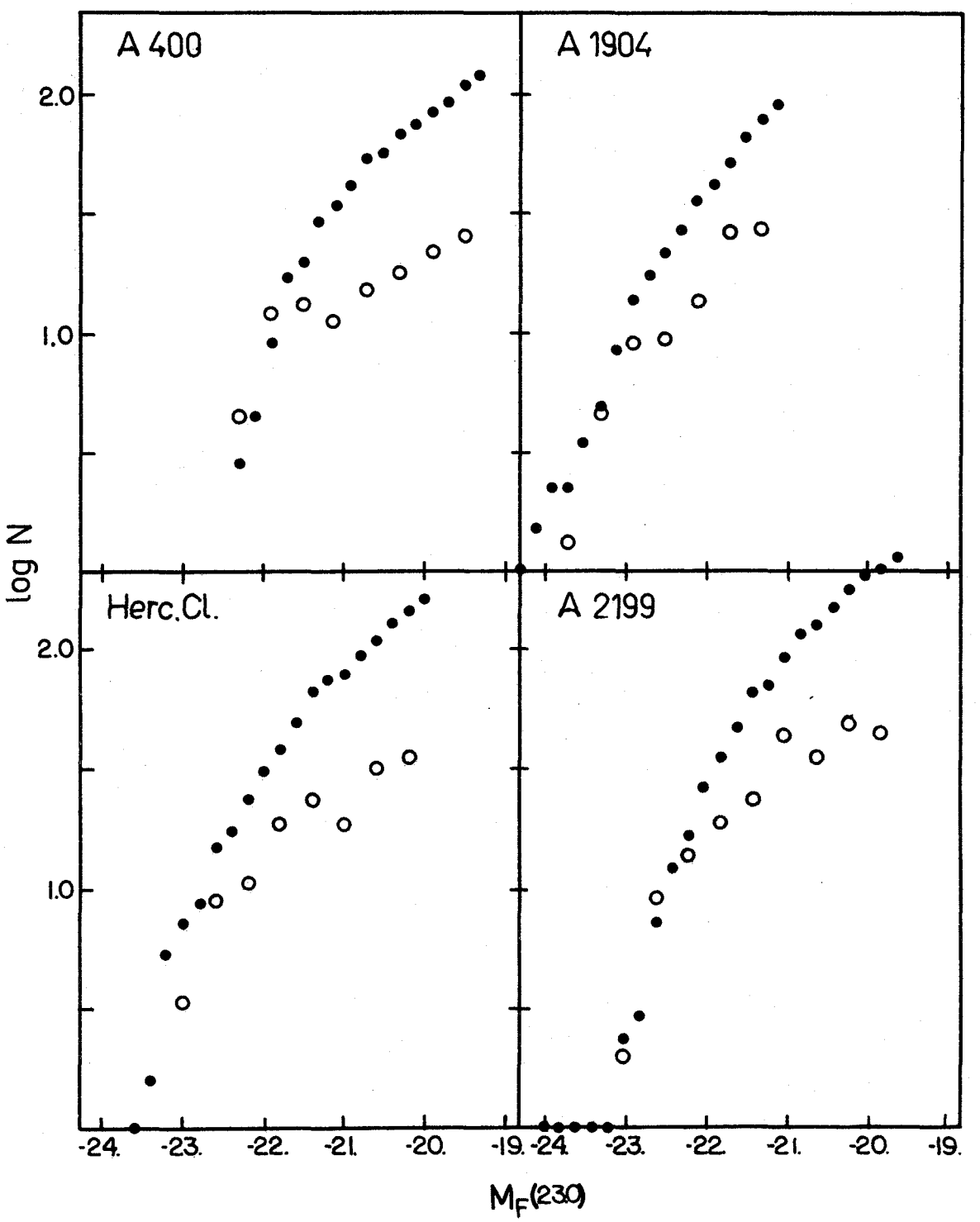

FIGURE 6.- continued

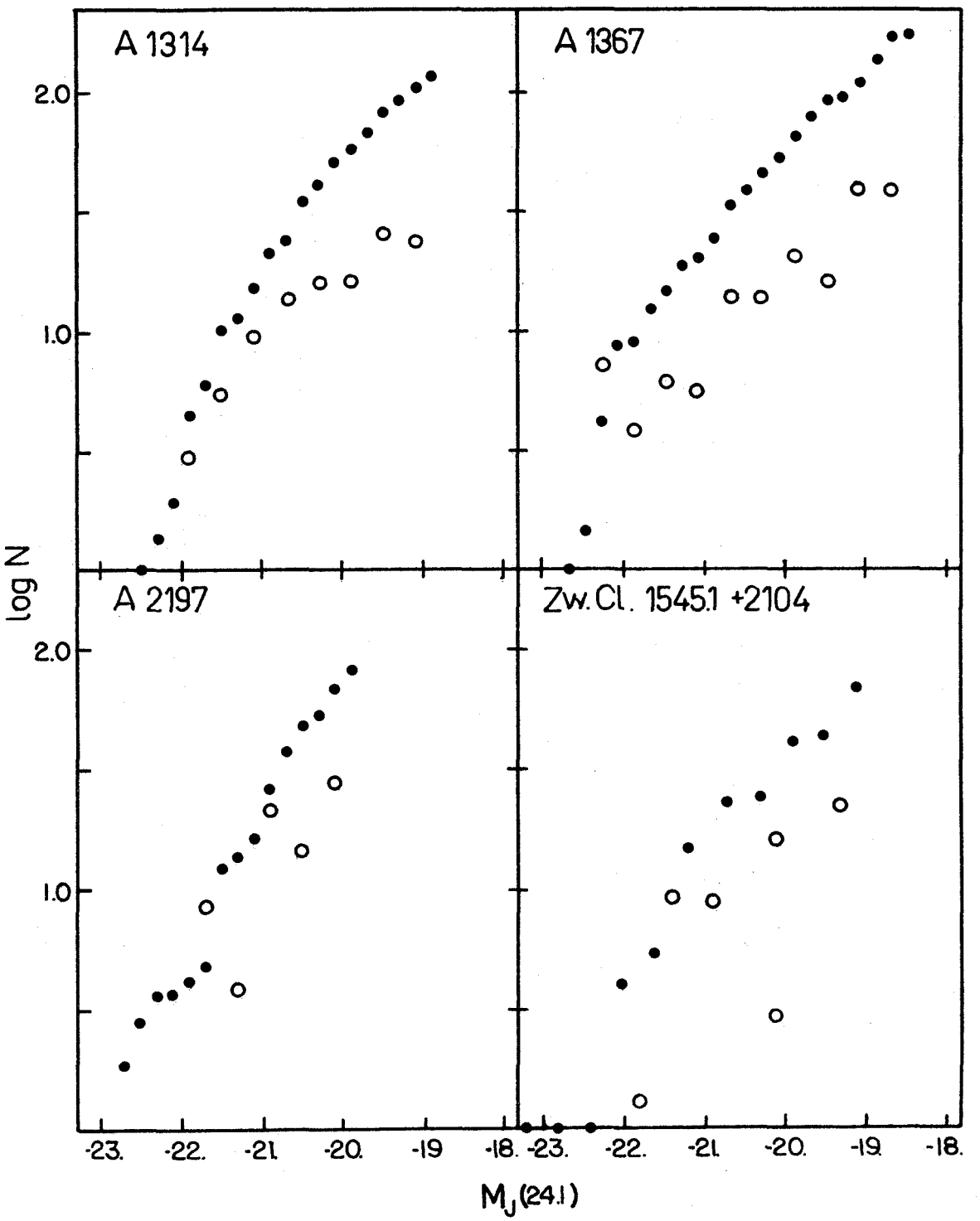

FIGURE 6.- continued

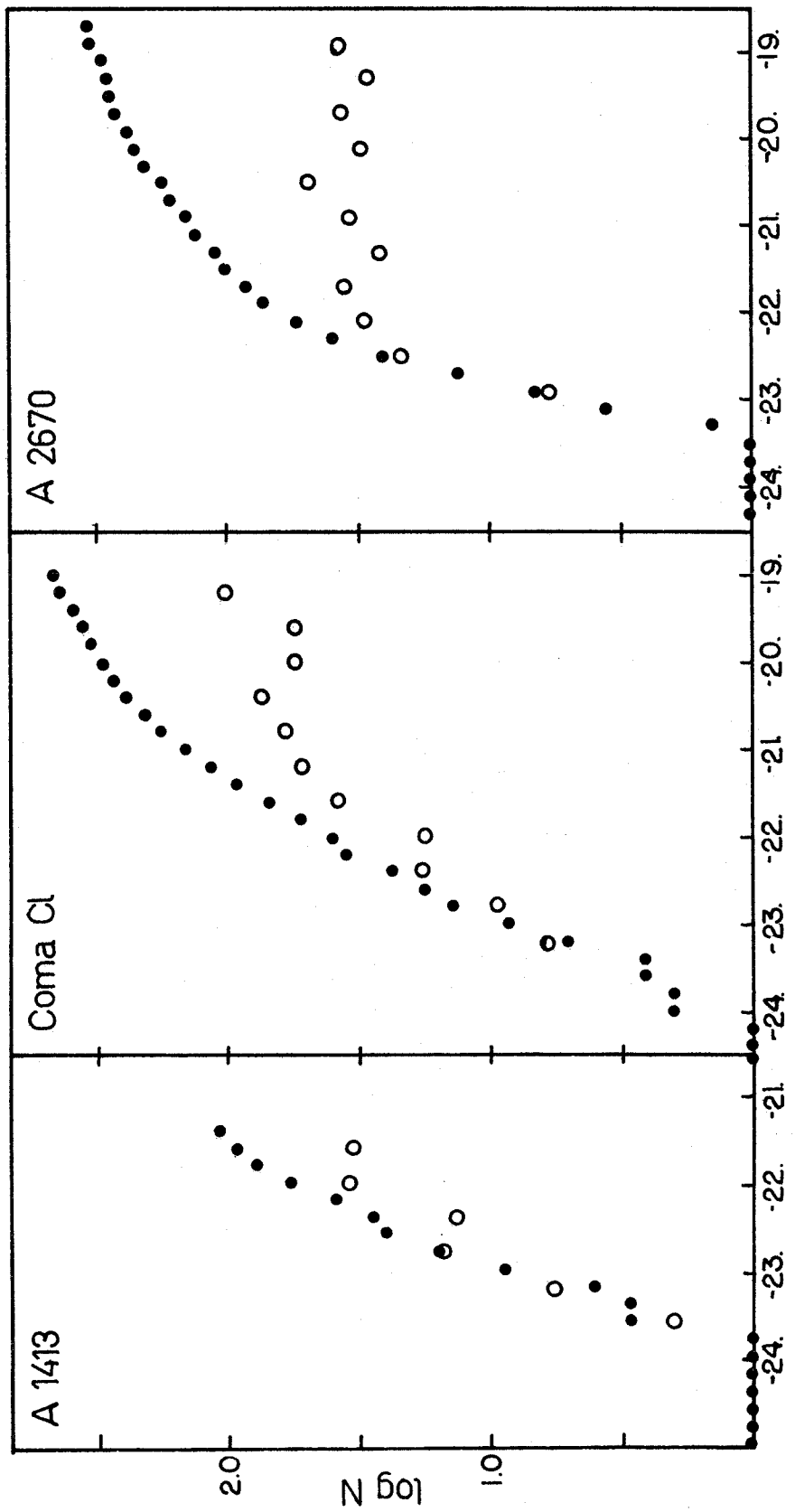

FIGURE 6.- continued

where the brightest galaxies form a long chain. However, circular symmetry must be assumed along the line of sight, anyway, and the number of objects is too small to adequately specify any other shape for the distribution in the plane of the sky.

In each cluster, the center was determined by visual inspection and the total surface brightness due to galaxies calculated in a series of concentric rings. The largest field studied of each cluster, whose depths ranged from 2.5 to 4 mag beyond the brightest member, was used for this purpose. Then the surface brightness due to background objects, calculated from Figure 4, was subtracted and a series of corrections made. The effect of galactic absorption was removed using equations 6 and 7. Extrapolations from isophotal to total magnitude were made using the relation in Figure 5. The additional luminosity in galaxies beyond the completeness limit of the large field was added using the cluster luminosity function, extrapolated to infinite magnitude by

$$\log N = C + 0.15 \cdot m \qquad (8)$$

The luminosities were converted to the visual band using $J - V = 0.0$ and $J - F = 1.1$ for spiral poor clusters or $J - F = 0.9$ for spiral rich clusters (A 1228, A 1367, A 2197, and the Hercules cluster). The surface brightnesses of distant clusters are corrected for the effect of the k factor

and the redshift-angular diameter relation for $q_o = 0.0$.

The final results are presented in Figure 7. The horizontal scale is in megaparsecs and the vertical scale in units of 20 mag per square arc minute, which is equivalent to $9.62 \times 10^{10}\ L_\odot Mpc^{-2}$. The error bars are the sum of the uncertainties due to Poisson statistics and the assumed 50 percent uncertainty in the background.

The accuracy of these profiles deteriorates rapidly at large radii, where the background galaxies are dominant. Rather than relying on individual points in analyzing these profiles, the outer parts have been fit to a power law $s \sim r^{-3.0}$, which is the best fit to the sum of all the profiles and is the relation predicted by the models to be discussed in the next section. Using this curve and a smooth fit to the inner points, the total luminosity was calculated for each cluster. To make the results for A 2670 comparable with those for the other clusters, the diffuse background light, amounting to one third the entire cluster luminosity (Oemler 1973), has been omitted.

Then using Von Zeipel's inversion to obtain the three dimensional mass distribution, the binding energy can be calculated for a given mass luminosity ratio. In the second and third columns of Table 2 are listed, for each cluster, the total luminosity, in solar units, and the gravitational radius, R_G, in megaparsecs, the latter being defined by

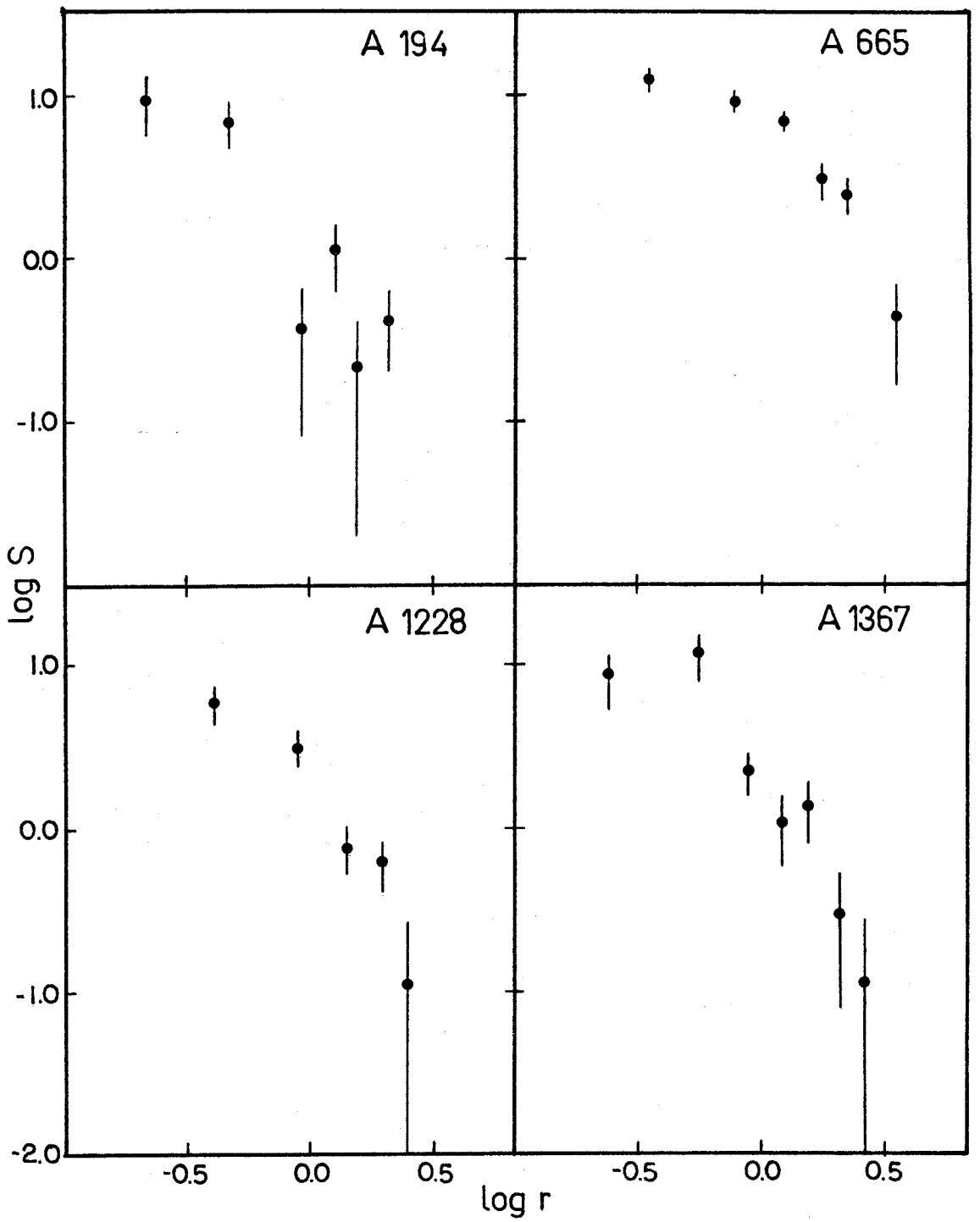

FIGURE 7.- Cluster surface brightness profiles. r is in megaparsecs and S in units of 20 mag per square minute in the V band.

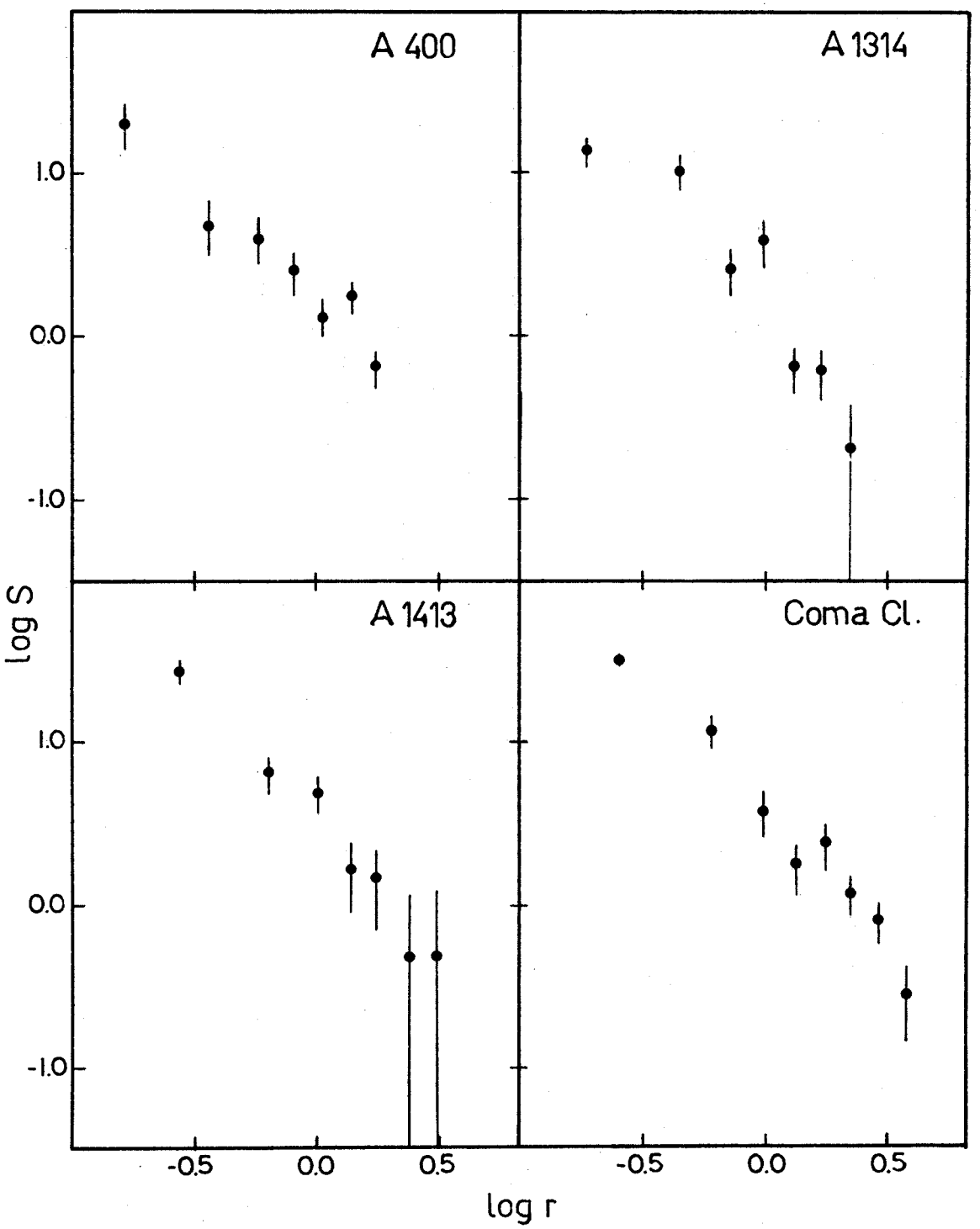

FIGURE 7.- continued

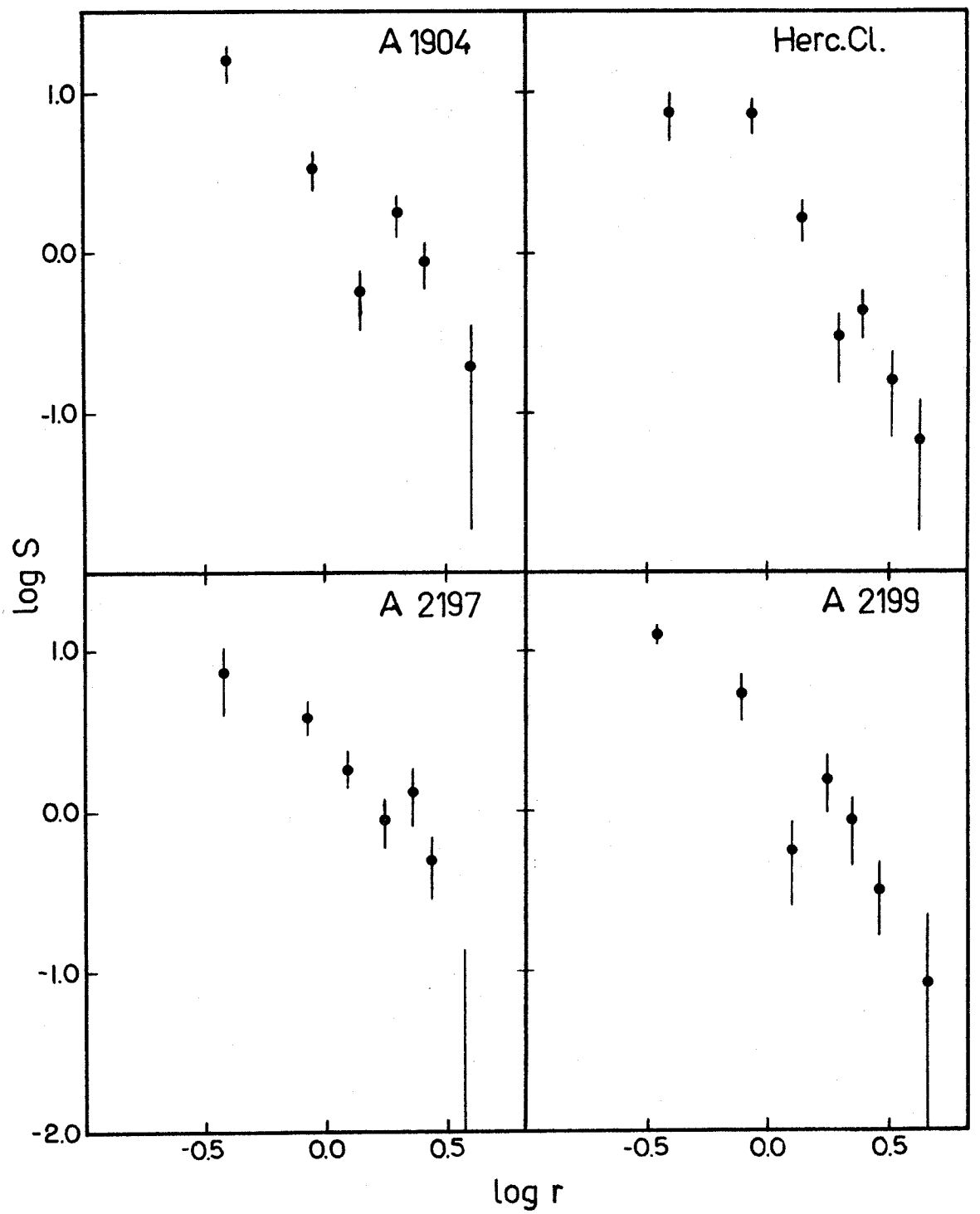

FIGURE 7.- continued

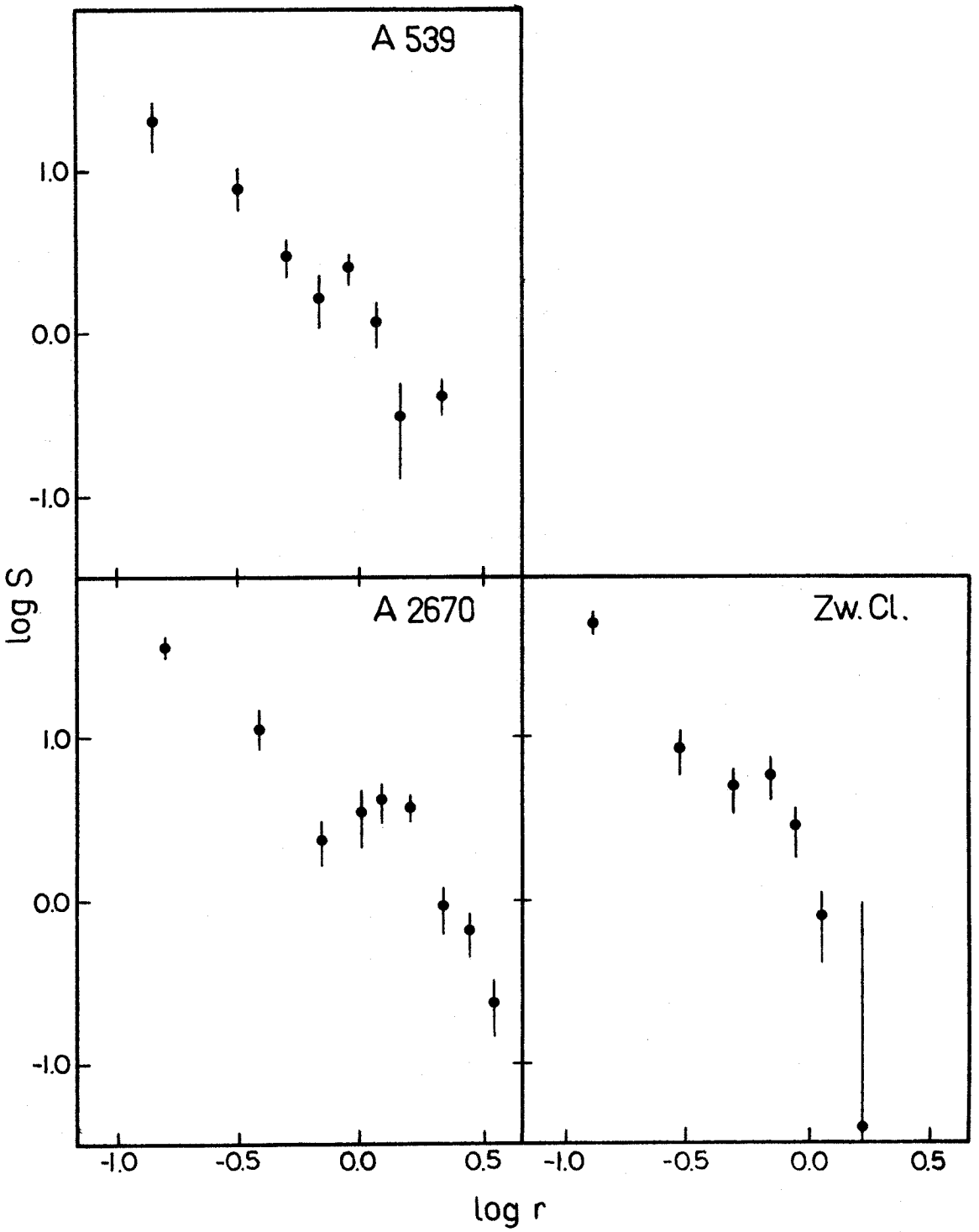

FIGURE 7.- continued

$$E_{Grav} = -\frac{GM^2}{R_G} \qquad (9)$$

For those clusters in which the morphological types of the galaxies were classified, the fractional composition of each type has been calculated for those galaxies within R_G and within 3 mag of the brightest member. These percentages are listed in the next three columns of Table 2.

TABLE 2

CLUSTER PARAMETERS

Cluster	L ($10^{12} L_\odot$)	R_G (Mpc)	%E	%S0	%Sp	$\langle \Delta v^2 \rangle^{\frac{1}{2}}$	M/L
Abell 194	1.8	2.6	18	56	26	782	203±47
Abell 400	3.5	3.3	15	56	29	359	28±15
Abell 539	2.6	2.7	19	53	28		
Abell 665	17.0	5.6					
Abell 1228	2.9	3.7	14	25	63		
Abell 1314	3.1	2.8	38	43	19	928	179±86
Abell 1367	3.3	2.9	17	40	43		
Abell 1413	8.2	3.4					
Coma cluster	9.4	3.9	35	47	18	1430	195±38
Abell 1904	7.8	4.0					
Hercules cluster	3.6	4.0	14	36	50	1232 (749)	388±136 (143±50)
Abell 2197	4.2	4.1	19	36	45	490	54±25
Abell 2199	5.7	3.7	35	41	24	1092	178±49
Abell 2670	5.5	3.7				1525	360±165
Zw Cl 1545.1 +2104	2.6	2.6					

d) Numerical Models

In analyzing the information contained in Figures 6 and 7 and Table 2, it will be very helpful to have available theoretical models, to compare with the observations and to supply certain information which is unobtainable observationally. The best models of clusters of galaxies extant are a series of numerical models which have been, very kindly, made available by Dr. S. J. Aarseth in advance of publication.

These calculations follow the dynamical evolution of a system of 100 objects, whose relative masses are proportional to the luminosities of the 100 brightest galaxies in the Coma cluster. At time t=0, the cluster is at rest at the point of maximum expansion. The points are scattered at random within a spherical volume with the small random velocities which they would have acquired during the previous expansion phase. The behavior over the succeeding 4.2 collapse times is illustrated in Figures 8 through 10. Figure 8 shows the ratio of gravitational to kinetic energy as a function of time, the horizontal coordinate being the time in units of the collapse time. The cluster rebounds partially after the initial collapse, then quickly settles down. The oscillations in the ratio of gravitational to kinetic energy have damped to less than 10 percent after 2 collapse times, and, after

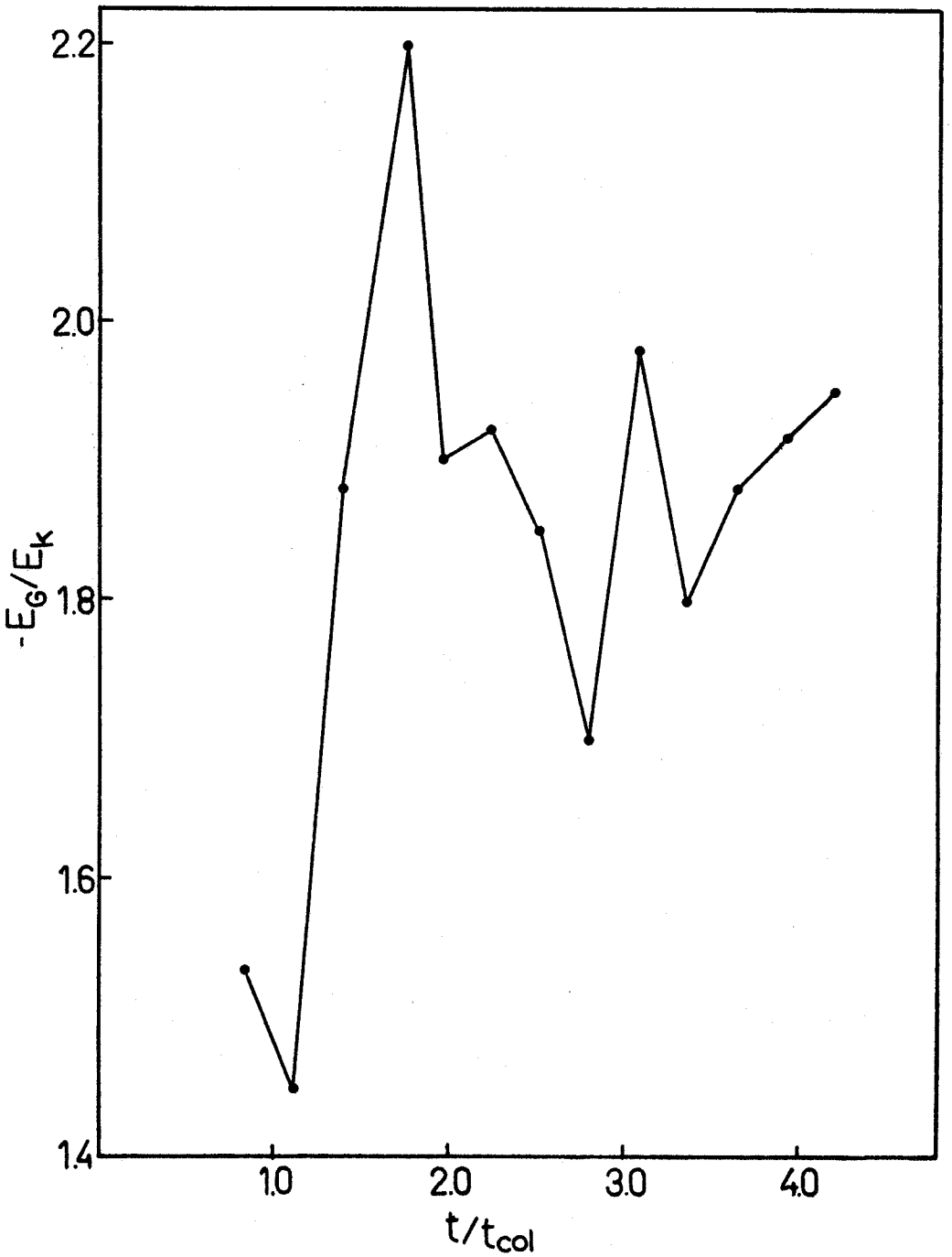

FIGURE 8.- The ratio of gravitational energy to kinetic energy as a function of time. The horizontal coordinate is the time in units of the collapse time.

4 collapse times, this ratio is only slightly below the steady state value of 2.0.

The evolution of the projected mass distribution is presented in Figure 9. Curve 1 is the sum of four models with $1.4 \leq t/t_{col} \geq 2.24$, curve 2 is the sum of four models with $2.52 \leq t/t_{col} \geq 3.36$ and curve 3 is the sum of three models with $3.64 \leq t/t_{col} \geq 4.20$. When $t/t_{col} = 1.40$, the outer envelope has already reached the distribution $S \sim r^{-3}$ which it will maintain. The central density gradient begins low and with increasing time approaches, but does not reach, the steep gradient of the outer envelope. Also presented in Figure 9, by the x's, is a numerical model by Peebles (1970) which represents a cluster of 300 equal mass objects averaged over the period from 2 to 4 collapse times. It fits in quite well with the sequence of Aarseth models, and shows the same r^{-3} envelope profile. However, it appears to be less evolved than the Aarseth models at the same dynamical time, perhaps because the large number of equal mass objects inhibits two body relaxation. It is worth noting that none of these models approximates an isothermal sphere, whose projected density follows a r^{-1} law.

Violent relaxation is very important in the early evolution of the system, but two body relaxation should be much less effective, because of its longer time scale. In Figure 10 there is presented, for the same three groups of models as

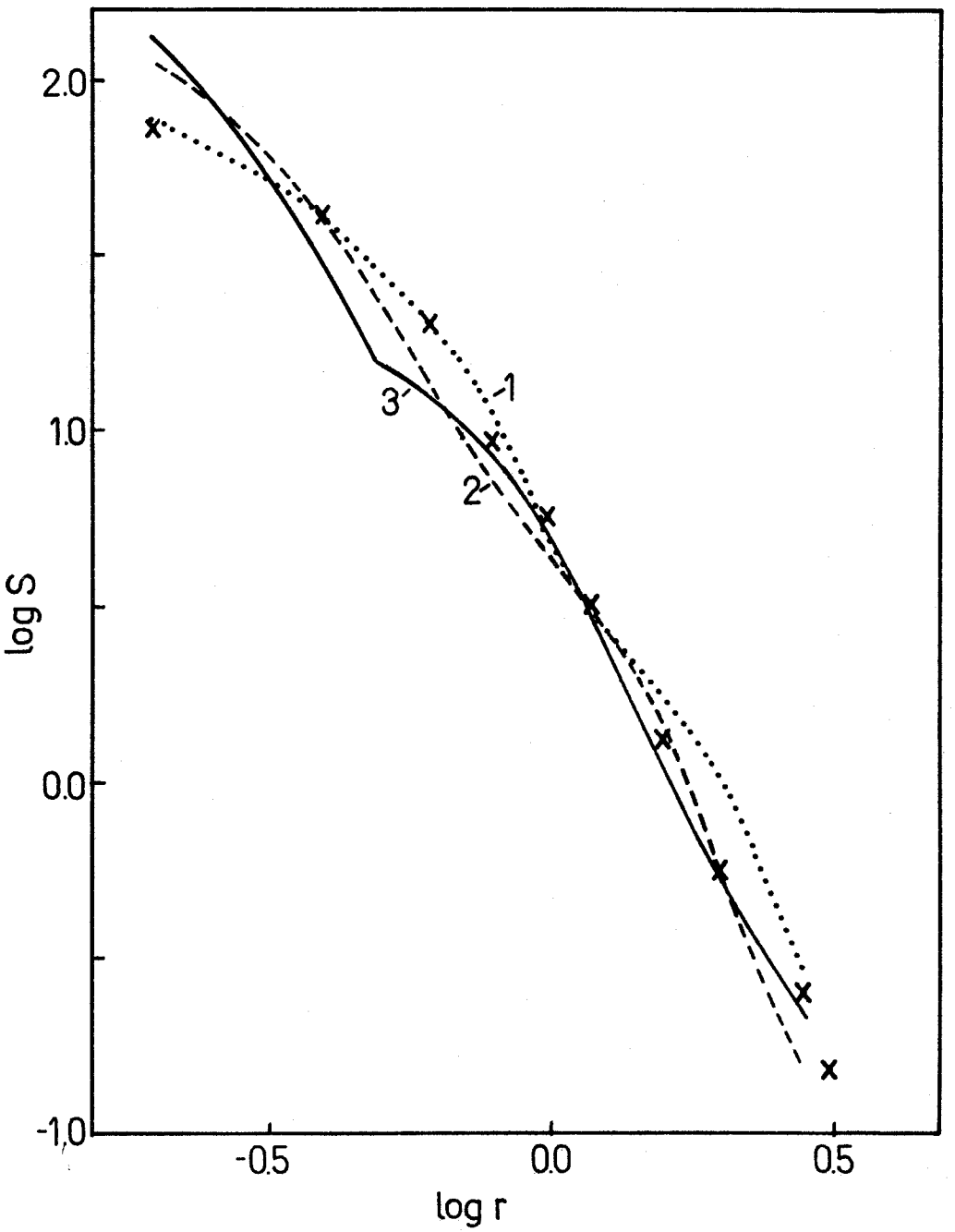

FIGURE 9.- The three profiles are each the mean of several Aarseth models. Curve 1: $1.4 \leq t/t_{col} \leq 2.24$; Curve 2: $2.52 \leq t/t_{col} \leq 3.36$; Curve 3: $3.64 \leq t/t_{col} \leq 4.2$. The x's represent the mean of Peebles's models with $2 \leq t/t_{col} \leq 4$.

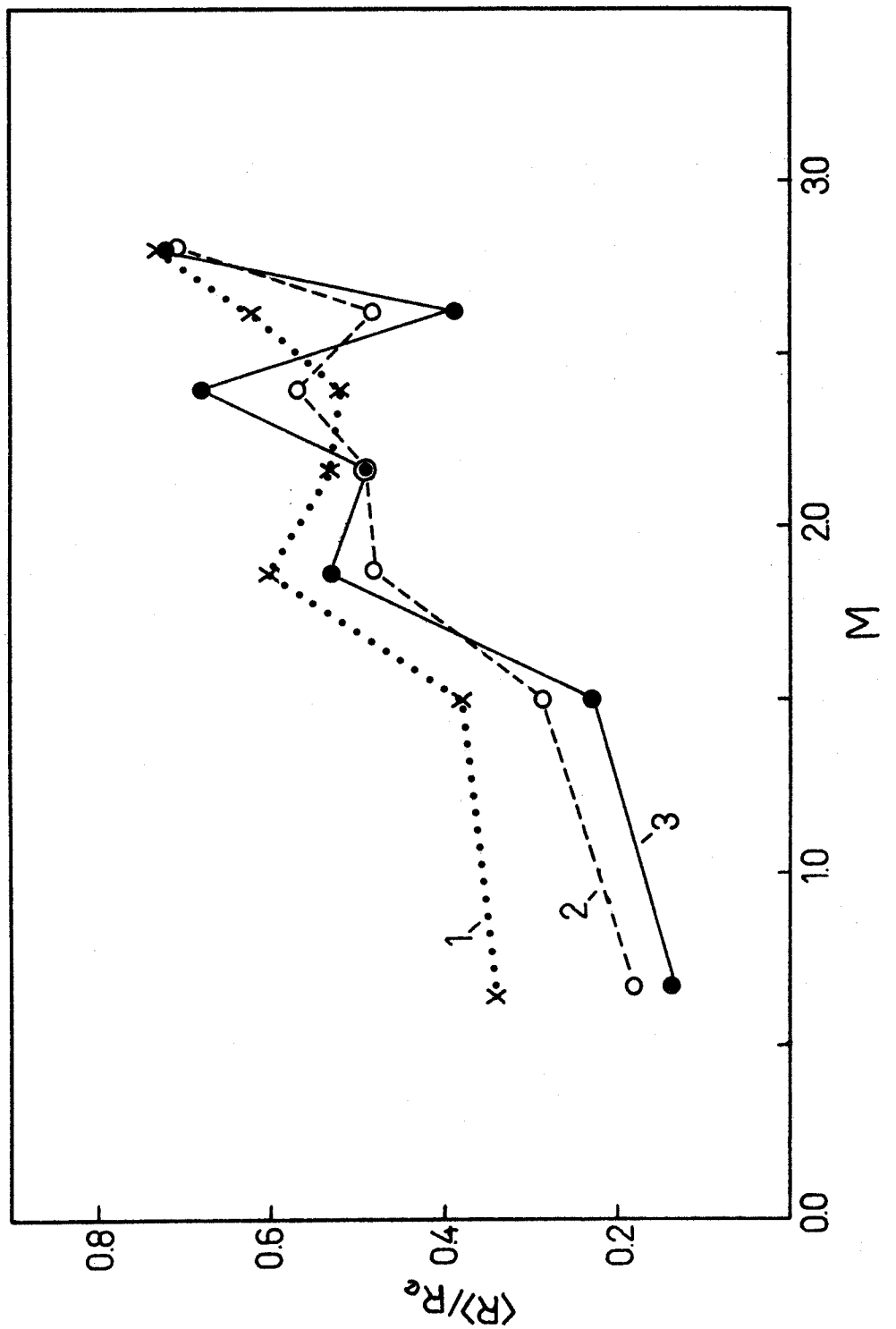

FIGURE 10.- The ratio of the mean radius of objects within R_G to that for a constant density distribution, as a function of magnitude. The curves refer to the same groups of models as in Figure 9.

in Figure 9, the ratio of the mean projected radius of objects within the projected gravitational radius to that for a constant density distribution. The objects are grouped in magnitude intervals assuming a constant mass to light ratio and a magnitude of 0.0 for the most massive object. The heaviest objects, corresponding to NGC 4889 and NGC 4874 in the Coma cluster, quickly fall to the center. As time passes, the slightly smaller objects also lose energy by two body interactions and move inward. However, even in the last models, the galaxies more than 2.0 mag fainter than the brightest have undergone only slight relaxation. It is interesting that, despite the mass segregation among the heavier objects, there is no observable trend of velocity dispersion with mass.

To calculate mass to light ratios for clusters we will need to know the relation between the line of sight velocity dispersion and the total kinetic energy per unit mass. In Figure 11, the quantity k, defined by

$$k = \frac{E_k}{1/2\ m < v_{los}^2 >} \qquad (10)$$

is presented as a function of projected radius for the same three groups of models as in previous figures. As there appears to be no clear trend of this relation with time, the mean solid curve will be adopted for all clusters.

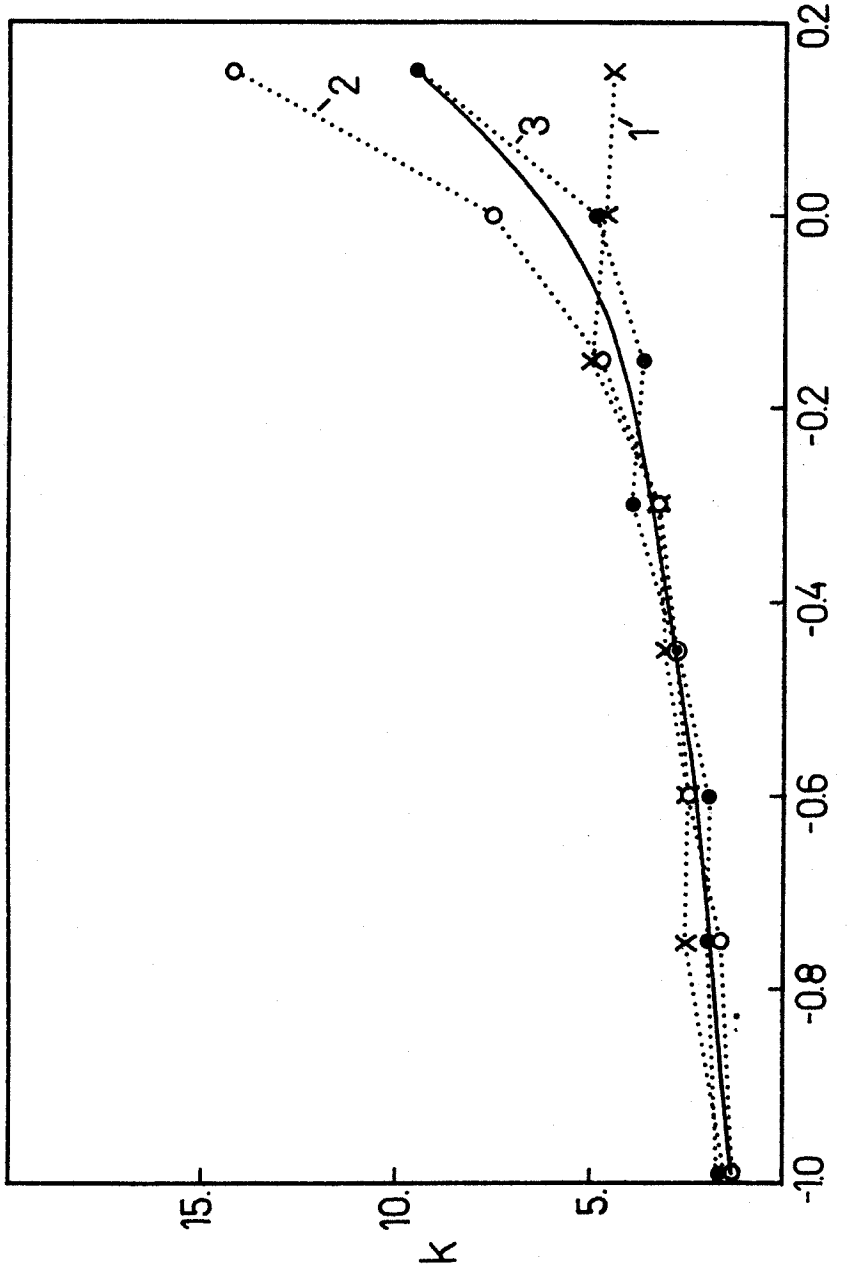

FIGURE 11.- The ratio, k, of the total kinetic energy per unit mass to that inferred from the line of sight velocity dispersion, for the same Aarseth models as in previous figures. The solid line is the adopted relation for all clusters.

IV. CLUSTER VELOCITY DISPERSIONS

In studying the structure and dynamics of these fifteen clusters, the profiles in Figure 7 will be most useful if the luminosity can be converted into mass. Although most clusters have dynamical times measured in billions of years, Figure 8 assures us that, even after only 2 collapse times, the cluster mass can be fairly reliably obtained from the internal velocity dispersion by application of the virial theorem.

There exist in the literature sufficient galaxy redshifts to calculate velocity dispersions of five of the clusters in this study: A 194, the Coma cluster, the Hercules cluster, A 2197 and A 2199. To supplement these data, observations were made of galaxies in a number of additional clusters using the cassegrain image tube spectrographs on the Palomar 200-inch and 60-inch telescopes. Sufficient good quality spectra were obtained of galaxies in three clusters A 400, A 1314, and A 2670. The A 2670 data are presented in Oemler (1973). In Table 3, the galaxies in A 400 and A 1314 are listed along with their NGC/IC numbers, 1950 coordinates, magnitudes, projected distances from the center, in arc minutes, and the telescope with which they were observed.

The 200-inch spectra have a dispersion of 190 Å mm^{-1} and the 60-inch spectra a dispersion of 285 Å mm^{-1}. All

TABLE 3

NEW MEASUREMENTS OF GALAXY VELOCITIES

Cluster	NGC/IC	α(1950)	δ(1950)	$m_F(m_J)$	r(')	Tel.	v_{rad}
A 400		2 55.0	5 50	13.46	0.0	200	6900
		2 55.0	5 50	13.40	0.0	200	7280
		2 54.9	5 46	13.70	3.6	200	6970
		2 55.7	5 54	13.37	10.6	60	7330
		2 55.4	5 45	14.24	8.8	200	7440
		2 55.1	5 52	14.43	2.9	200	6940
		2 54.7	5 47	14 37	6.6	200	7650
		2 55.8	6 06	13.76	21.0	60	7510
A 1314	IC 712	11 32.1	49 21	(13.82)	0.0	60	9850
	IC 709	11 31.5	49 19	(14.56)	5.9	60	9550
	IC 708	11 31.2	49 20	(14.00)	8.2	60	9320
		11 30.9	49 12	(14.97)	14.0	60	10450
		11 30.6	49 23	(15.49)	16.0	60	9050
		11 33.9	49 20	(14.61)	18.0	60	9910
		11 33.8	49 24	(14.28)	17.0	60	11010
		11 29.4	49 17	(14.88)	26.0	60	9820
		11 30.8	49 31	(14.38)	16.0	60	10060

spectra were measured on the Caltech Grant machine and the measurements were reduced using the standard Caltech spectra reduction program. Lines used included Ca H and K, the G band, Hβ and unblended lines of FeI and MgI. The standard deviation of the calculated radial velocities, determined from the dispersion in redshift of individual lines, averaged 100 km s^{-1} for all clusters. These velocities, corrected for galactic rotation, are presented in the last column of Table 3.

Data on the Coma cluster were taken from Rood et al (1972) and on A 194 from Zwicky and Humason (1964). Observations of galaxies in A 2197, A 2199 and the Hercules cluster were gathered from several sources, and are summarized in Table 4 in the same format as Table 3. Where more than one reference is cited for a particular galaxy, the velocity listed is the average of the quoted values.

All measured redshifts were used to compute the velocity dispersion in A 2670, A 400, A 1314, A 2197 and A 2199. In the Coma cluster, only galaxies within 1° of the cluster center were used. Galaxies NGC 4858 and IC 3998, with velocities more than 3σ above the mean, were rejected as background objects. In A 194, 2 galaxies with velocities 5σ and 6σ above the mean were omitted for the same reason. In the Hercules cluster, the close pair NGC 6040, which were not in the Burbidge list, are 3σ higher than the mean. Since it

TABLE 4

PUBLISHED MEASUREMENTS OF GALAXY VELOCITIES

Cluster	NGC/IC	α(1950)	δ(1950)	$m_F(m_J)$	r(')	Ref.	v_{rad}
Hercules	NGC 6047	16 02.8	17 52	13.19	11.	B	9593
	NGC 6045	16 02.8	17 54	13.80	10.3	B	10001
	NGC 6044	16 02.7	18 00	13.98	10.	B	10059
	IC 1183	16 03.3	17 54	14.08	4.1	B	10161
	IC 1181A	16 03.2	17 44	13.20	16.	B	10477
	NGC 6041	16 02.3	17 51	12.87	18.	B	10561
	IC 1185	16 03.5	17 51		10.	B	10575
	IC 1181B	16 03.2	17 44	14.47	17.	B	10813
	IC 1173	16 02.9	17 32	14.50	28.	B	10963
	IC 1186	16 03.5	17 28	14.28	30.	B	11135
	NGC 6050A	16 03.1	17 54	14.00	7.8	B	11179
	NGC 6061	16 04.0	18 22	13.27	24.	B	11294
	NGC 6055	16 03.2	18 17	13.51	18.	B	11314
	IC 1194	16 04.4	17 54		17.	B	11763
	NGC 6056	16 03.4	18 03	14.57	4.3	B	11781
	NGC 6040E	16 02.1	17 53	13.22	19.	C2	12740
	NGC 6040W	16 02.1	17 53	13.69	19.	C2	12508
A 2197		16 24.2	40 28	(15.20)	45.	C1	8952
	NGC 6160	16 26.0	41 02	(13.99)	17.	C1	9545
		16 26.8	41 20	(14.61)	25.	C1	8704
	NGC 6173	16 28.1	40 55	(13.40)	8.	C1	8929
		16 28.9	41 36	(14.71)	43.	C1	9276
		16 32.4	41 27		50.	C1	8888
		16 27.7	40 59	(15.27)	53.	C2	8385
		16 28.7	41 02	(15.27)	17.	C2	9296
		16 28.8	40 50	(14.82)	17.	C2	9104

TABLE 4 (cont.)

Cluster	NGC/IC	α(1950)	δ(1950)	$m_F(m_J)$	r(')	Ref.	v_{rad}
A 2197	NGC 6180	16 28.9	40 40	(14.70)	24.	C2	9314
A 2199		16 25.3	39 26	14.83	24.	K	9227
		16 25.4	39 38	14.06	18.	K	10168
	NGC 6158	16 26.0	39 30	13.35	15.	K	9083
		16 24.6	40 05	14.07	37.	C1	9222
		16 25.9	39 23	15.89	21.	C1	10712
	NGC 6166A	16 26.9	39 40	12.20	0.	M	9480
	NGC 6166B	16 26.9	39 40		0.	M	7960
	NGC 6166C	16 26.9	39 40		0.	M	10050
		16 26.7	39 41	14.29	3.1	M	9070
		16 26.7	39 43	15.07	4.2	M	9690
		16 26.8	39 38	14.50	2.2	M	10400
		16 26.8	39 40	15.43	1.0	M	10090
		16 26.9	39 39	17.16	2.8	M	8610
		16 26.9	39 38	14.51	2.0	M	7850
		16 27.0	39 35	13.80	4.9	M	9360
		16 27.0	39 36	15.87	4.2	M	10270
		16 27.0	39 38	15.15	2.5	M	8510
		16 27.0	39 30	14.48	7.0	M	10740
		16 27.0	39 45	16.03	5.3	M	8780
		16 27.0	39 35	14.81	5.5	M	7790
		16 27.0	39 39	15.61	2.0	M	8460
		16 27.0	39 41	15.77	3.9	M	8300
		16 27.0	39 46	15.80	7.2	M	9220
		16 27.1	39 46	15.80	7.3	M	8210
		16 27.1	39 44	15.59	4.3	M	8410

TABLE 4 (cont.)

Cluster	NGC/IC	α(1950)	δ(1950)	$m_F(m_J)$	r(')	Ref.	v_{rad}
A 2199		16 27.2	39 41	15.19	2.8	M,C2	8966
		16 27.3	39 37	15.18	6.5	M	8840
		16 27.3	39 48	15.42	9.6	C2	8315

References:

B Burbidge and Burbidge (1959)
C1 Chincarini and Rood (1972a)
C2 Chincarini and Rood (1972b)
M Minkowski (1961)
K Kintner (1971)

is not clear whether they should be included, the calculations will be performed both with and without them.

To calculate the three dimensional velocity dispersion of a cluster, the square of the deviation of each galaxy velocity from the mean was multiplied by the appropriate factor from Figure 11. The resulting values of $\langle \Delta v^2 \rangle^{\frac{1}{2}}$ for all clusters are listed in the seventh column of Table 2. In some cases, these differ significantly from what would have been obtained using a single value of k for all clusters.

Finally, using the virial theorem, the mass-luminosity ratios listed in the last column of Table 2 were calculated by

$$\frac{M}{L} = \frac{R_G \langle \Delta v^2 \rangle}{G \cdot L} \qquad (11)$$

The uncertainty in the velocity dispersion of n galaxies was obtained from the χ^2 distribution with n-1 degrees of freedom.

V. ANALYSIS OF THE RESULTS

A few points are immediately obvious from inspection of Figures 6 and 7. All of the luminosity functions are roughly similar in shape and could be fit, with varying degrees of success, to the suggested standard curves of either Abell (1962) or Press and Schechter (1974). Most of the cD clusters stand out because of the exceptionally bright first ranked member, but the absolute magnitude of the steep part of the luminosity function is similar in all of the clusters. Nevertheless, there are some significant differences between individual clusters.

Similarly, each of the profiles in Figure 7 has some resemblance to at least one of the models in Figure 9. But, in some of the profiles, particularly in those of the cD clusters, there is a dip or plateau at about 1 Mpc which was not expected from the theories.

To make any progress in understanding these results, the data must be ordered in some way. Clusters of galaxies have been classified by a number of systems; one of the most natural and objective methods is by their galaxy content. Inspection of Table 2 and the descriptions in §IId shows that they divide into three groups. The cD clusters have one (or two, in the case of Coma) unique and dominant member and have E:S0:Sp ratios of about 3:4:2; this group includes

A 1413, the Coma cluster, A 1904, A 2199, A 2670 and Zw Cl 1545.1 +2104. The spiral rich clusters have an E:S0:Sp ratio of about 1:2:3 and include A 1228, A 1367, the Hercules cluster and A 2197. The remaining clusters, which may be called spiral poor, have E:S0:Sp ratios of about 1:2:1 and include A 194, A 400, A 539, A 1314 and A 665. The classification of A 665 is uncertain because of its distance, but its appearance suggests that it belongs to the third rather than the second class. With the exception of A 1314, whose proportions of galaxy types resemble those of the cD clusters, there is no ambiguity in the typing of any of these clusters.

There is a strong correlation between these groupings and the general appearance of the clusters. Spiral rich clusters tend to be irregular in shape, with no symmetry and no apparent gradient in density towards the center. On the other hand, the cD clusters tend to resemble globular star clusters, being rather circular, with a well defined center towards which the mass is highly concentrated. The spiral poor clusters fall midway between these two types, being more regular than the spiral rich clusters but less regular than the cD clusters.

Composite differential luminosity functions for spiral rich, spiral poor and cD clusters are presented in Figures 12 through 14. The error bars represent the sum of the uncertainties (1σ) due to Poisson statistics and the uncertain

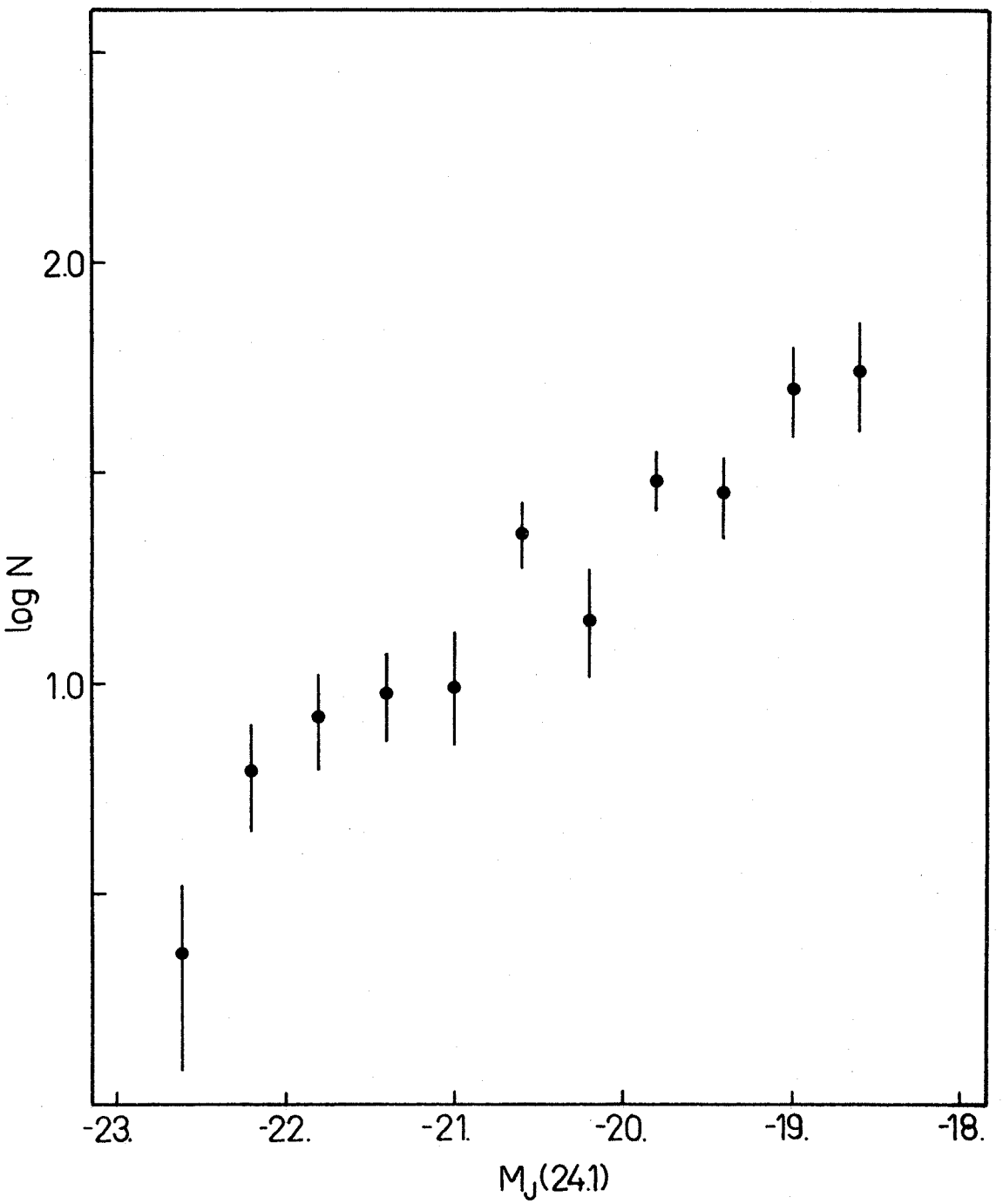

FIGURE 12.- Composite differential luminosity function for 3 spiral rich clusters, A 1228, A 1367 and the Hercules cluster. The error bars are due to statistics and the uncertainty in the background.

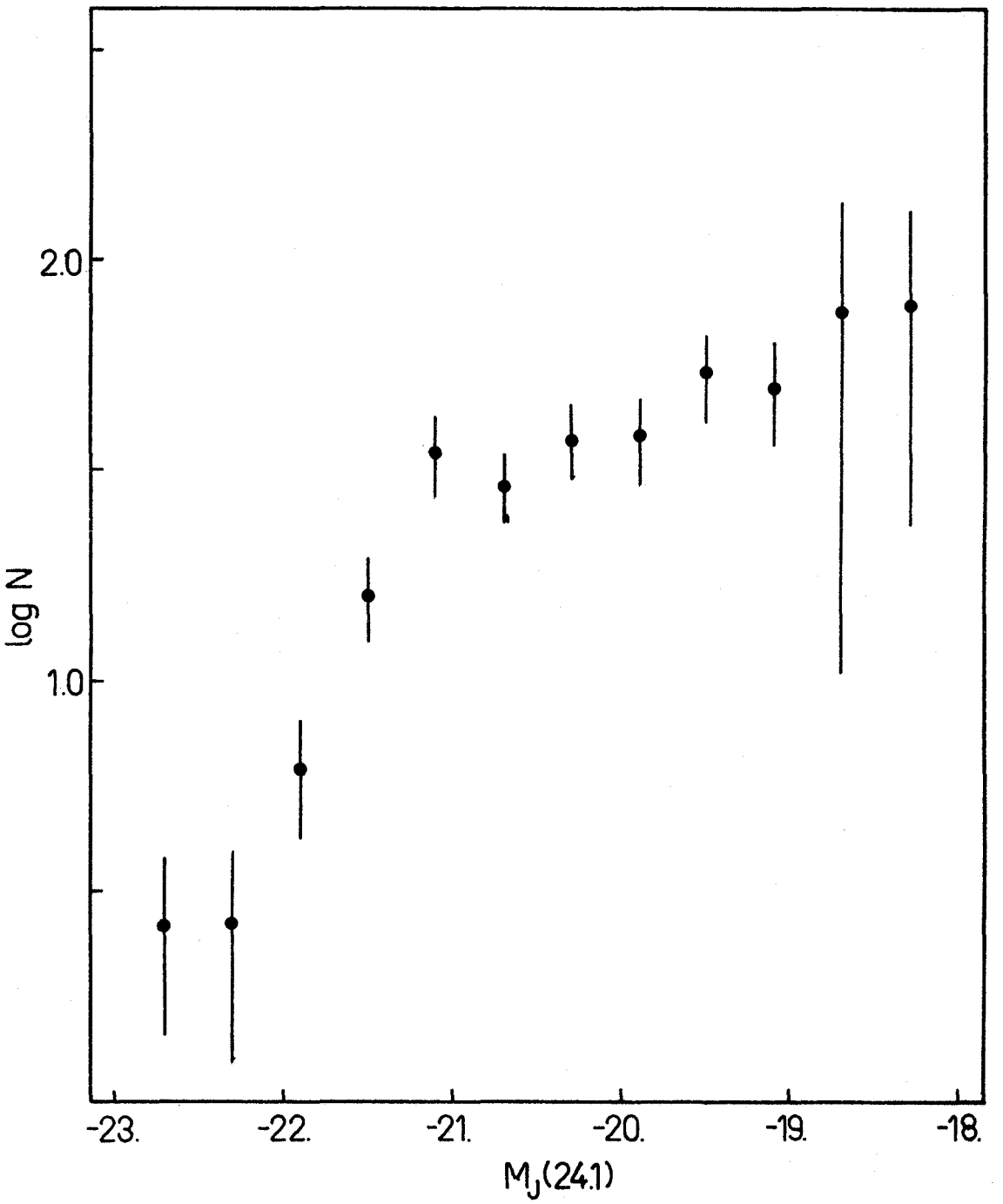

FIGURE 13.- Composite differential luminosity function for 3 spiral poor clusters, A 400, A 539 and A 1314.

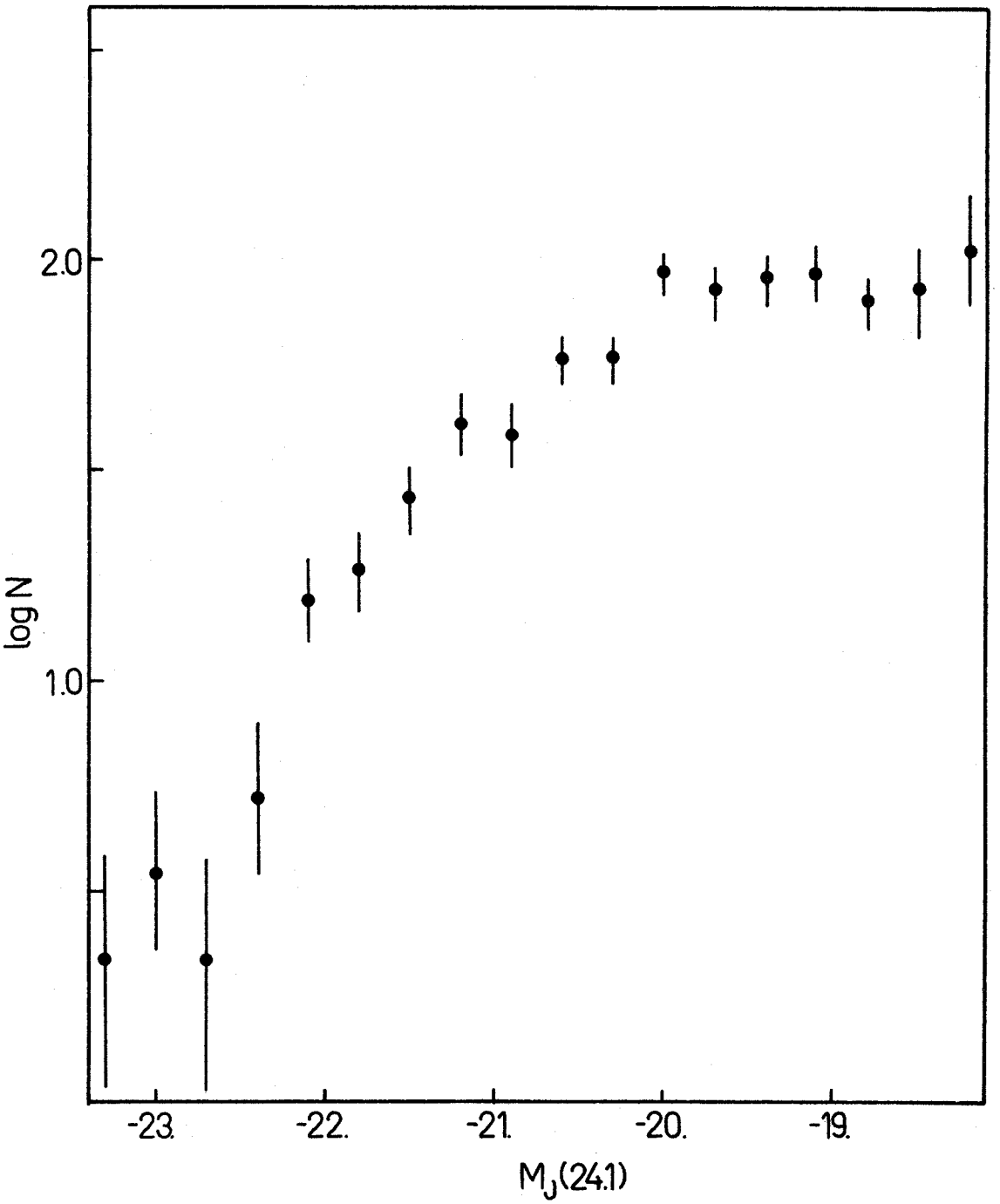

FIGURE 14.- Composite differential luminosity function for 4 cD clusters, A 1904, the Coma cluster, A 2199 and A 2670.

background corrections. The spiral rich luminosity function was constructed using A 1228, A 1367 and the Hercules cluster, the spiral poor luminosity function using A 400, A 539 and A 1314 and the cD luminosity function using A 1904, the Coma cluster, A 2199 and A 2670.

Except for the outstandingly bright first ranked member characteristic of the latter, the spiral poor and cD luminosity functions are identical to within the errors, and they differ significantly from that of the spiral rich clusters. This is not surprising; the compositions of the first two differ from each other by much less than the differ from that of the latter, and there is no reason to expect spiral, S0 and elliptical galaxies to have the same luminosity function. In fact, it is somewhat surprising that the absolute magnitude of the steep end of the spiral rich luminosity function is so close to that of the other two as this implies either that the mass-luminosity ratio of spirals is not appreciably different from those of ellipticals and S0's, or that the difference in M/L is quite closely cancelled by a difference in their mass functions.

Constructing a mean cD and spiral poor luminosity function and fitting it by eye to the luminosity functions of all clusters of these types gives a dispersion in absolute magnitude (assuming J-F=1.1) of 0.24 mag, which is not much larger than that expected from photometry errors and

uncertainty in the fitting. The mean luminosity function agrees quite well with that predicted theoretically by Press and Schechter (1974). The fit of two straight lines, suggested by Abell (1962) seems to be an oversimplification.

Two of these clusters, A 2670 and A 665, have conspicuously different luminosity functions for faint galaxies. Although they are both distant clusters, it is unlikely that the rapid flattening of their luminosity functions at the faint end is due to problems of completeness or background corrections at faint magnitudes. As they have little else in common, it is difficult to suggest any other possible cause.

The gravitational radius of each cluster, in megaparsecs, is plotted against its total luminosity, in solar units, in Figure 15. Spiral rich clusters are denoted by x's, spiral poor clusters by open circles and cD clusters by filled circles. Superimposed on the mean trend of size with luminosity is a systematic tendency for the spiral rich clusters to be larger and the cD clusters smaller than average. This reflects the earlier observation that spiral rich clusters are large and irregular, with no central concentration, while cD clusters are compact and centrally condensed.

Because of this variation of size with type, and because the various types are not distributed evenly with L, a single fit to all the data would be misleading. Instead, one straight line with a slope of 0.30 was fit by least squares to the

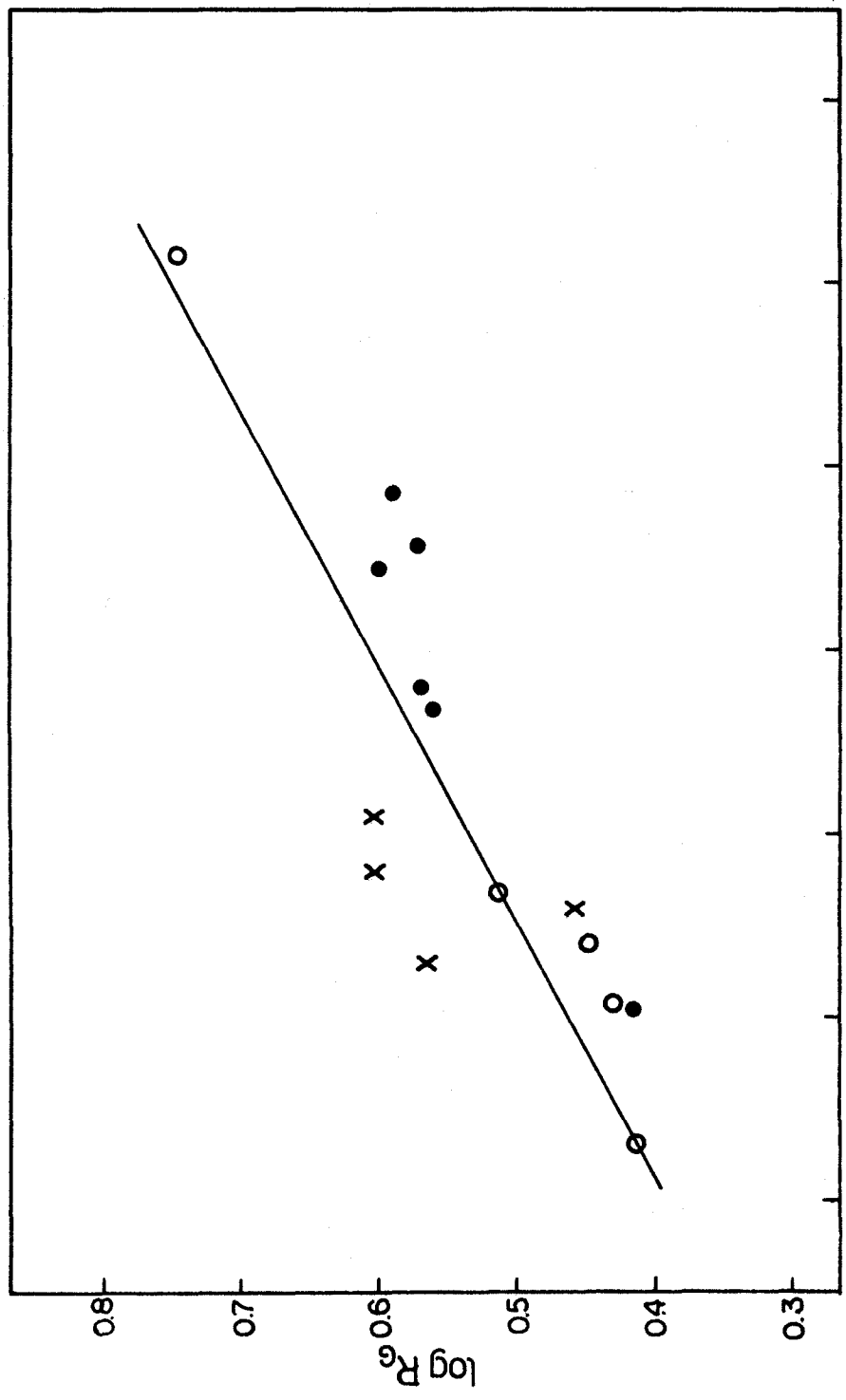

FIGURE 15.- Gravitational radius, in megaparsecs, versus total luminosity, in solar units, for all clusters. Spiral rich clusters are denoted by x's, spiral poor clusters by open circles and cD clusters by filled circles. The solid line is the fit to the data.

cD clusters and a separate line of slope 0.37 was fit to the rest of the data. The mean of these two lines, weighted by the number of clusters represented by each, is shown as a solid line in Figure 15. Its slope of 0.34 $\pm$ .05 is essentially equal to 1/3; in other words, in the mean all clusters have the same density, independent of mass. Therefore, these data are inconsistent with the relation $r \sim L^{0.5}$ which Fish (1964) found from a study of elliptical galaxies.

The systematic trend of size with type is illustrated in Figure 16a. Plotted for each cluster is the deviation of log R_G from the mean line versus its E:Sp ratio; A 2670 has been plotted, using an E:Sp ratio typical of cD clusters. With the exception of A 1367, which on plates is noticeably compact for a spiral rich cluster, there is a quite narrow relation between compactness and galaxy content.

In Figure 16b, the mass luminosity ratios from Table 2 are plotted against the E:Sp ratio for each cluster, the higher of the two values being plotted for the Hercules cluster. The three cD clusters, A 2199, A 2670 and the Coma cluster, and the one other cluster with similar galaxy content, A 1314, all have mass-luminosity ratios consistent with 225, as does one intermediate-type cluster, A 194. The problems posed by the other three clusters will be considered later.

The same groups of clusters used to construct the

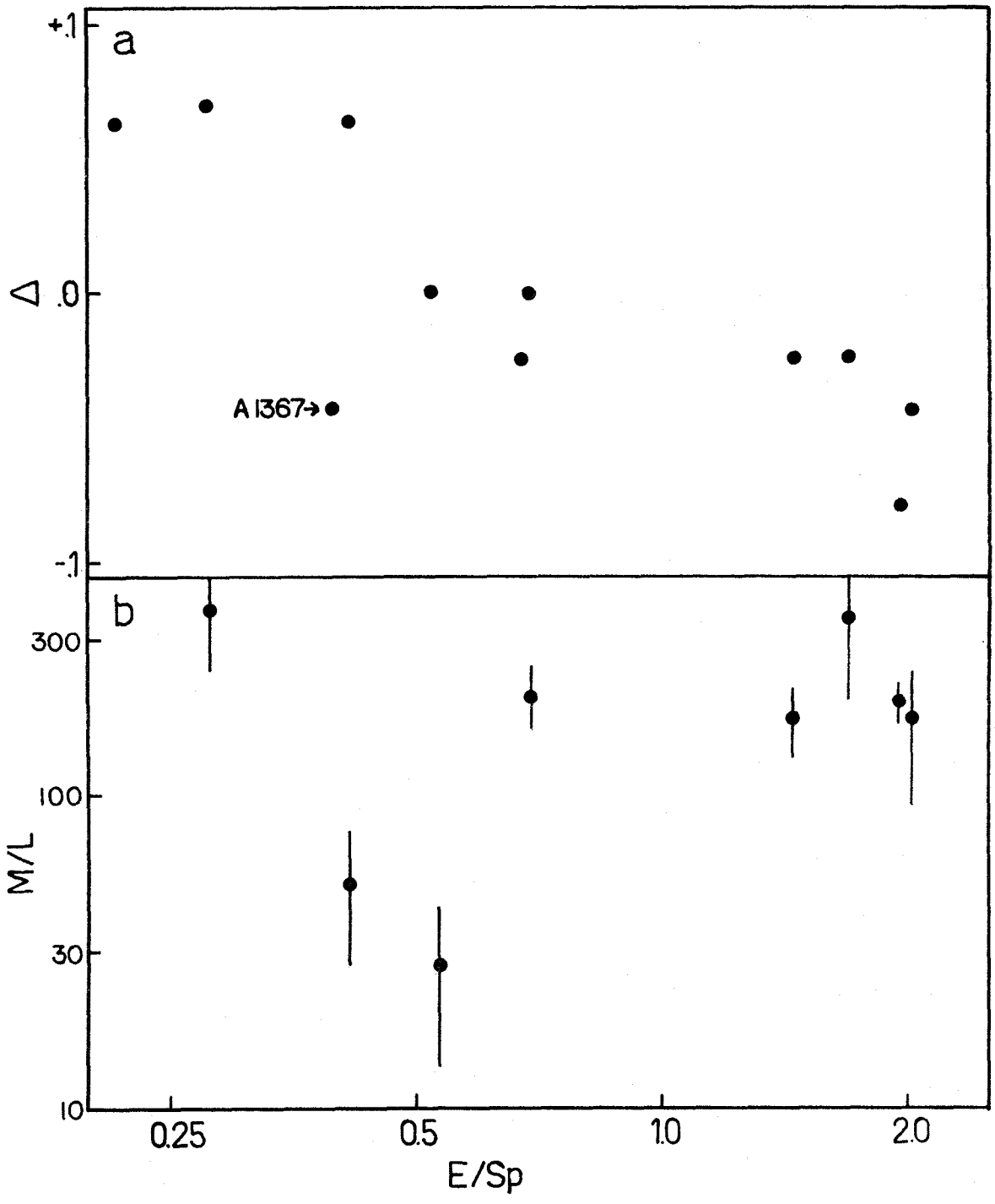

FIGURE 16.- a) The deviation of log R_G of a cluster from the mean line in Fig. 15 versus its elliptical to spiral ratio b) The mass-luminosity ratio of each cluster versus its elliptical to spiral ratio.

composite luminosity functions have been used to construct the mean profiles in Figures 17 through 19. Each cluster has been scaled by R_G^{-1} to equalize their size. Again, the errors are due to Poisson statistics and the background uncertainty. The vertical scale is in arbitrary units of surface brightness and the horizontal scale is the radius in units of R_G.

The outer envelopes of the spiral poor and cD profiles have the slope of approximately 3.0 expected theoretically, and the cores can each be fit to one of the family of models in Figure 9. Although they are quite similar, the cD cluster core seems to have a slightly higher luminosity gradient than the spiral poor core, and therefore would correspond to a slightly later model. This impression is reinforced by inspection of the individual profiles in Figure 7. The envelope of the spiral rich profile is poorly determined, although consistent with the models, but the core is too flat for even the earliest model. However, in all of these profiles there is a feature at about $0.4 \cdot R_G$ which grows in importance as one moves from spiral rich to spiral poor to cD clusters and which is totally unexpected.

The bump in the spiral rich profile might be ignored if it did not correspond to features in the other two profiles which cannot be ignored. The statistics are too poor to tell whether this feature is a plateau or a true local minimum. The dip in the composite cD profile is much smaller than that

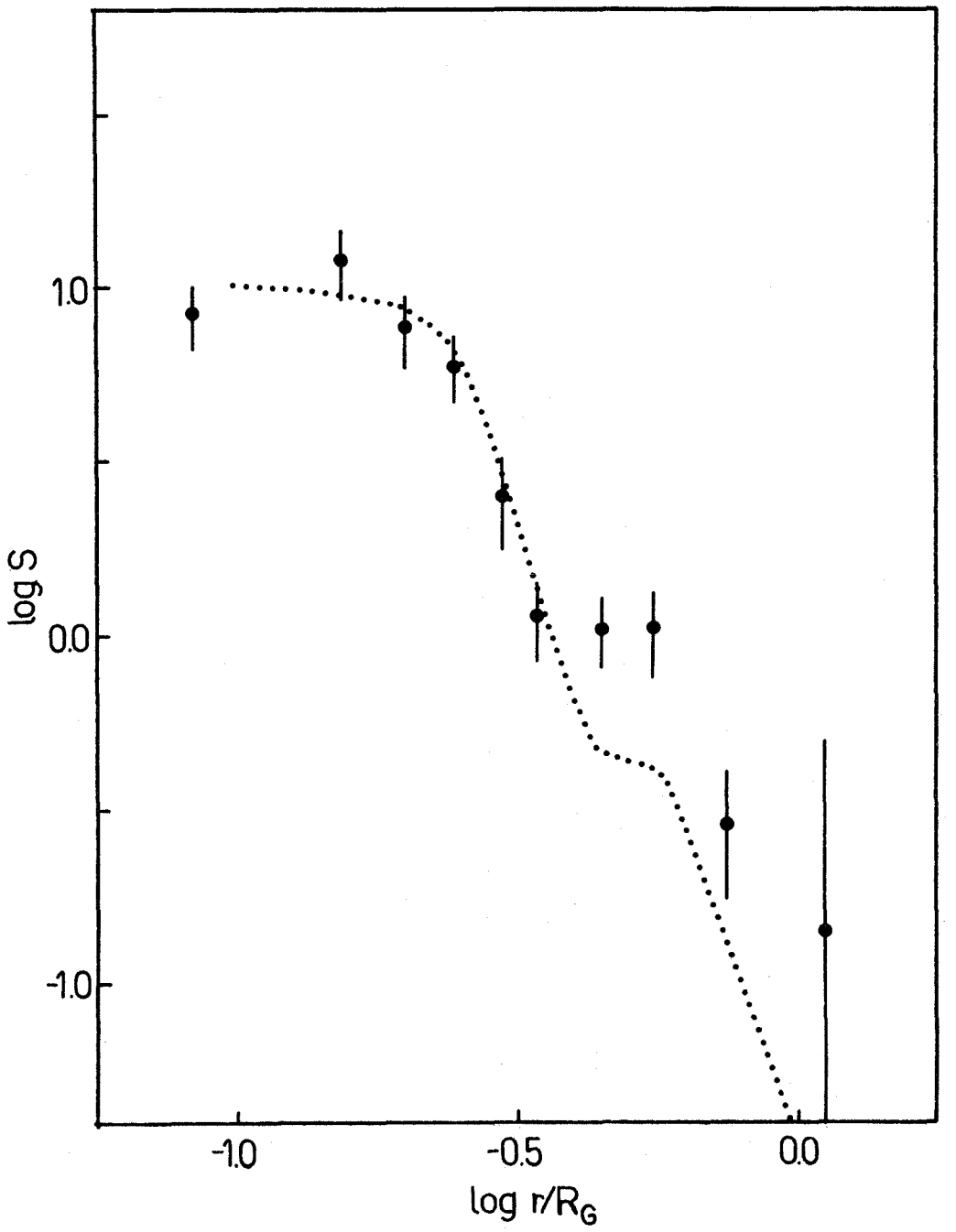

FIGURE 17.- Composite surface brightness profile of 3 spiral rich clusters A 1228, A 1367 and the Hercules cluster. The dotted line is a typical 3 dimensional mass distribution obtained from inverting a smooth curve through the points.

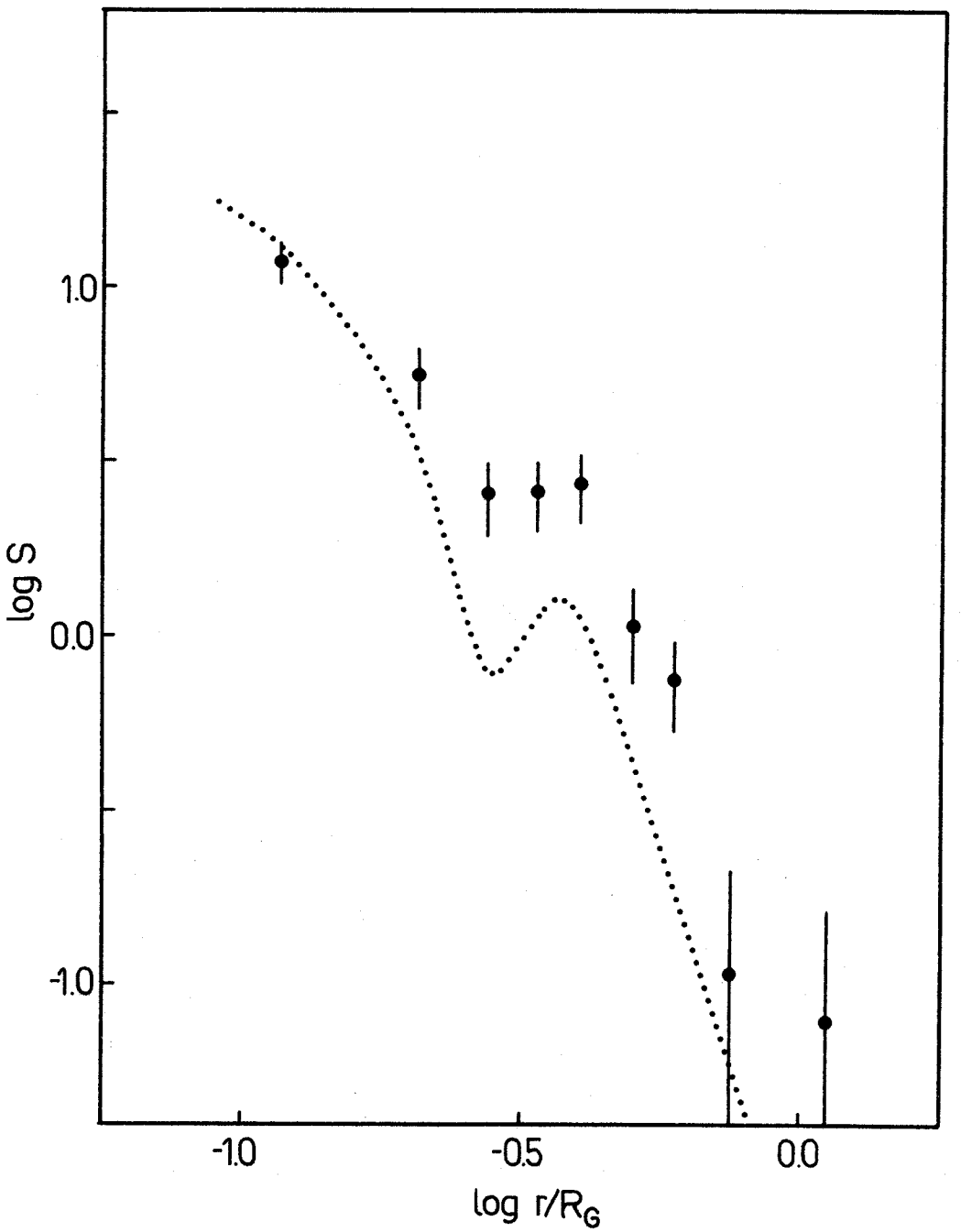

FIGURE 18.- Composite surface brightness profile for 3 spiral poor clusters A 400, A 539 and A 1314. The dotted line is a typical 3 dimensional mass distribution obtained from inverting a smooth curve through the points.

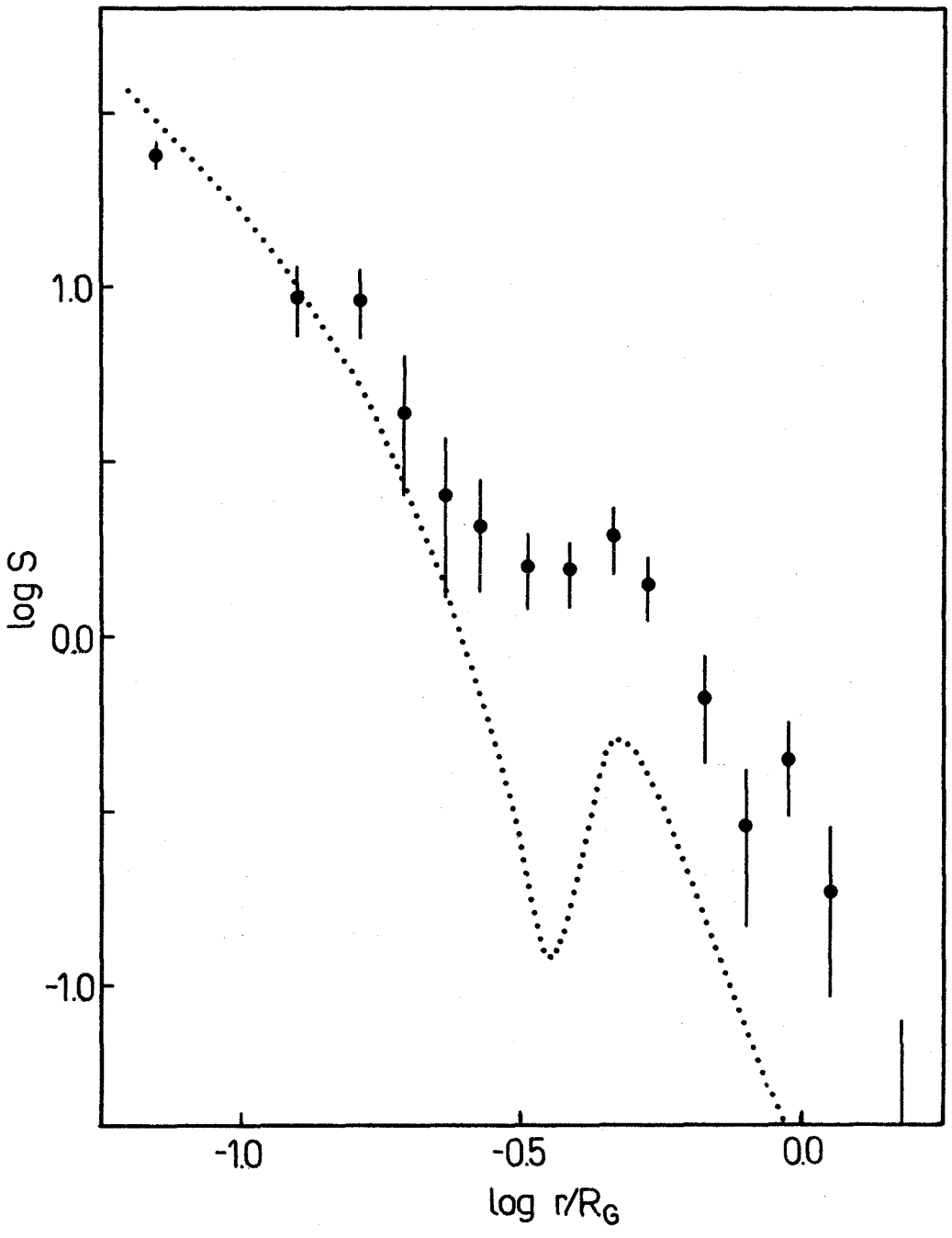

FIGURE 19.- Composite surface brightness profile for 4 cD clusters A 1904, the Coma cluster, A 2199 and A 2670. The dotted line is a typical 3 dimensional mass distribution obtained from inverting a smooth curve through the points.

in some individual cD cluster profiles- e.g. A 2199, A 1904, A 2670 - but whether this is due to improved statistics or the smearing of real feature by improper addition is unclear.

Even a modest plateau in the surface brightness profile can become a very disturbing hole in the space density distribution. The dotted curves in Figures 17 through 19 are typical three dimensional mass distributions obtained by inverting a smooth curve through the points. They are fairly reliable near both ends, but the solution near the feature is very sensitive to the exact profile adopted. One could easily draw a profile for the cD clusters which would make the volume density zero in some shell.

This feature has been seen by other investigators and cannot be easily explained away. Bahcall (1971) has shown that it is not due to measuring errors or the presence of subclustering. It is seen in both the luminosity distribution and number counts (Clark 1968). Since both of these depend on the brightness of the galaxies, one might wish to reconcile the observed profile with a smooth mass distribution by invoking a discontinuity in the mass to light ratio. This could be accomplished either by giving the galaxies in the core a higher mass-luminosity ratio or by removing mass from their outer envelopes into a diffuse sea of stars, where it would not be observed with the techniques used. It is known that such a component of diffuse light exists in some

clusters (Oemler 1973), but it is probably not massive enough. Also, a comparison of galaxies in the Coma cluster inside the feature (but excluding the very center) with those outside shows no difference in either their surface brightness or mean magnitude greater than 0.02 mag. From the information now available, we must conclude that this is a real feature in the mass distribution in clusters.

The composite cluster profiles have been broken down by the morphological types of the galaxies in Figures 20 through 22. These graphs are in the same format as Figures 17 through 19 except that the vertical axis represents number density rather than surface brightness. Although the uncertainties are large, the different galaxy types seem to have almost the same distribution, with one major exception: in the spiral poor and cD clusters, the projected density of spiral galaxies decreases towards the center. There is some suggestion, in the cD clusters, that the gradient of the elliptical density in the envelope is greater than the mean and that of the spirals less than the mean, but the statistical significance of this is rather low. Also in the cD profile, the ellipticals seem to participate the most, and the spirals the least, in the feature at 0.5 R_G.

The ratio of the mean radius of objects within R_G to that for a constant density distribution is presented, as a function of magnitude, for galaxies in spiral rich (1),

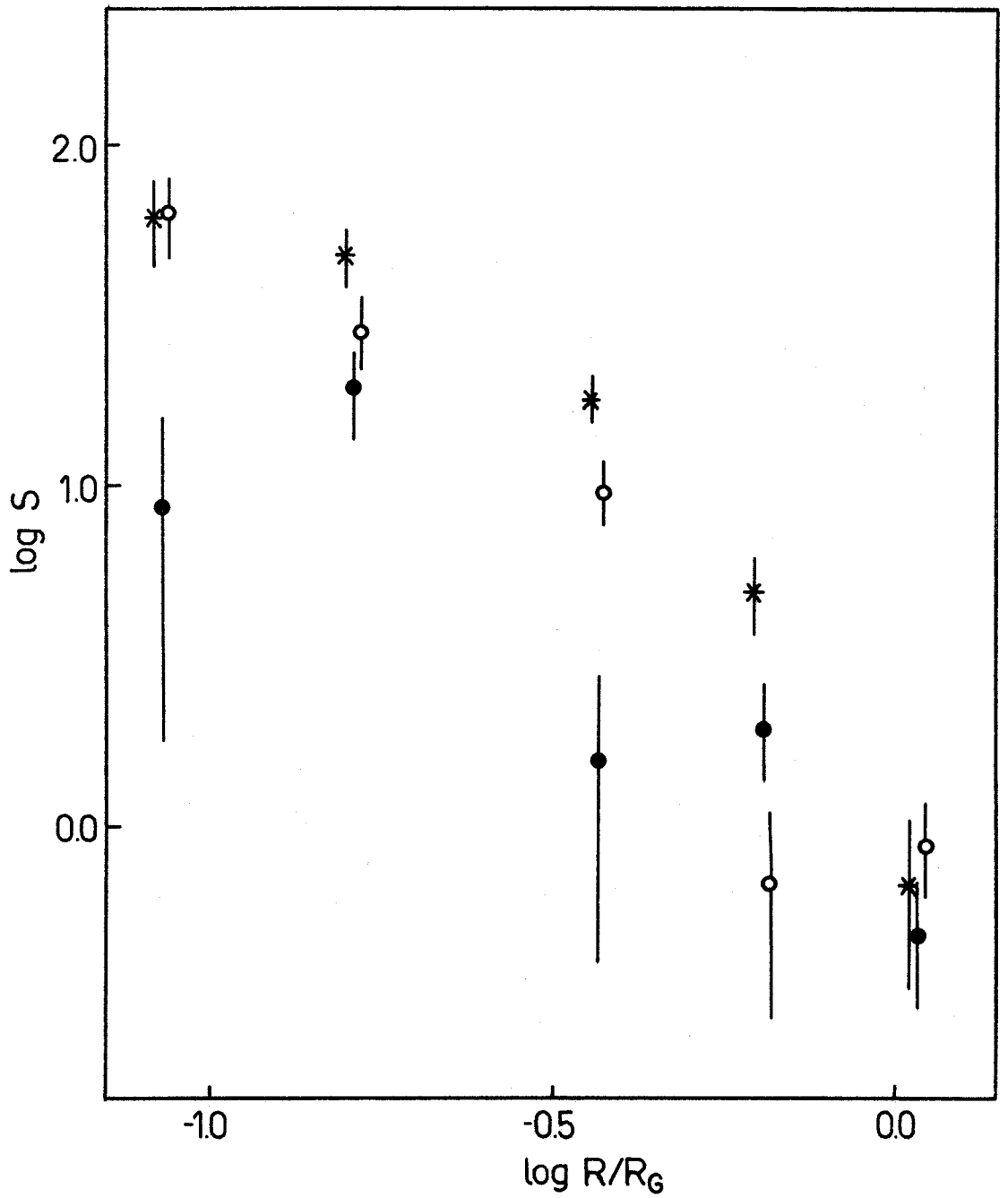

FIGURE 20.- Surface density of spirals (stars), S0's (open circles) and ellipticals (filled circles) in three spiral rich clusters A 1228, A 1367 and the Hercules cluster.

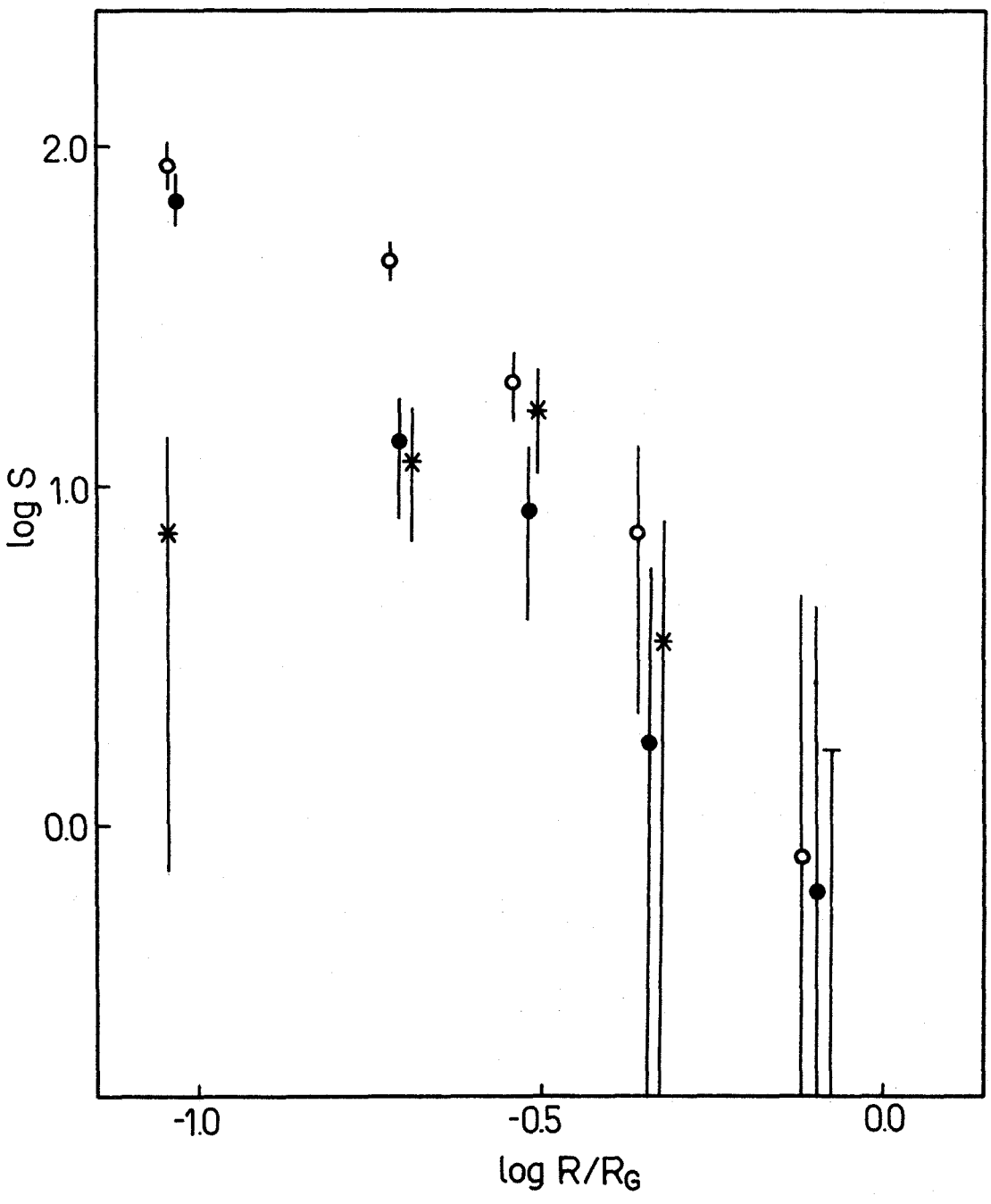

FIGURE 21.- Surface density of spirals (stars), S0's (open circles) and ellipticals (filled circles) in three spiral poor clusters A400, A 539 and A 1314.

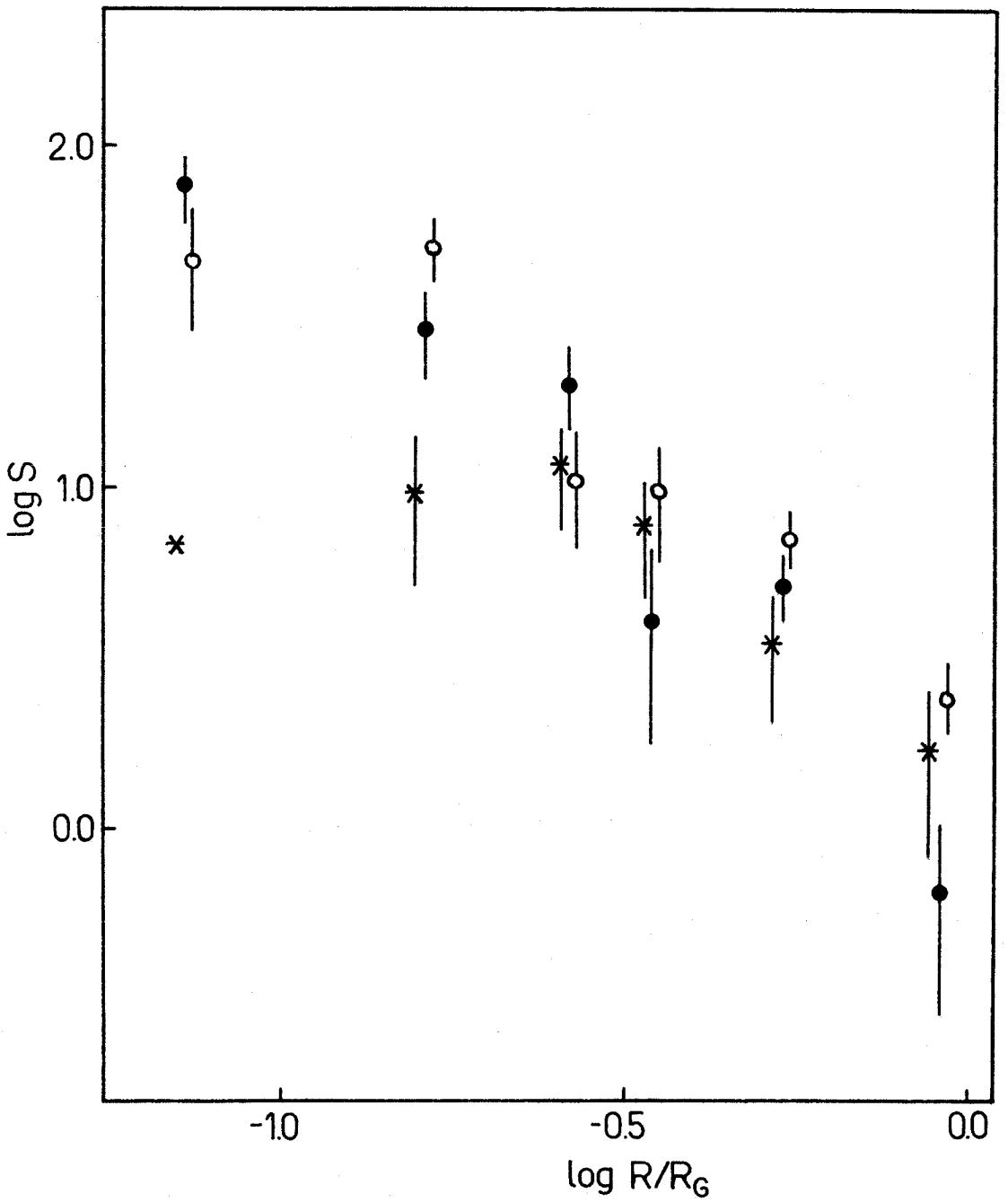

FIGURE 22.- Surface density of spirals (stars), S0's (open circles) and ellipticals (filled circles) in two cD clusters A 2199 and the Coma cluster.

spiral poor (2), and cD clusters (3) in Figure 23. As in the corresponding graph for the Aarseth models, in Figure 10, the magnitudes are normalized so that M = 0.0 for NGC 4889. The spiral rich clusters show no relaxation at all, but the other two types show mass segregation at the bright end of a magnitude similar to that in the models. There appears to be no relaxation by objects more than 2.0 mag fainter than the brightest galaxy. It is this result which validates our procedure of inferring the faint galaxy content of an entire cluster from photometry of galaxies near the center.

The comparison between Figures 10 and 23 has great significance for the distribution of mass in clusters. Two body relaxation in a system depends on the "graininess" of the gravitational field, and the qualitative similarity of the relaxation time in the models and real clusters means that the distribution of mass must also be similar. In particular, most of the mass in clusters must be located in the galaxies themselves, in rough proportion to their luminosities, rather than in some cluster-wide medium such as ionized gas or rocks. That the models show some slight relaxation even among the fainter galaxies while the real clusters do not can probably be attributed to the absence, in the former, of the many faint galaxies whose presence tends to smooth the gravitational field.

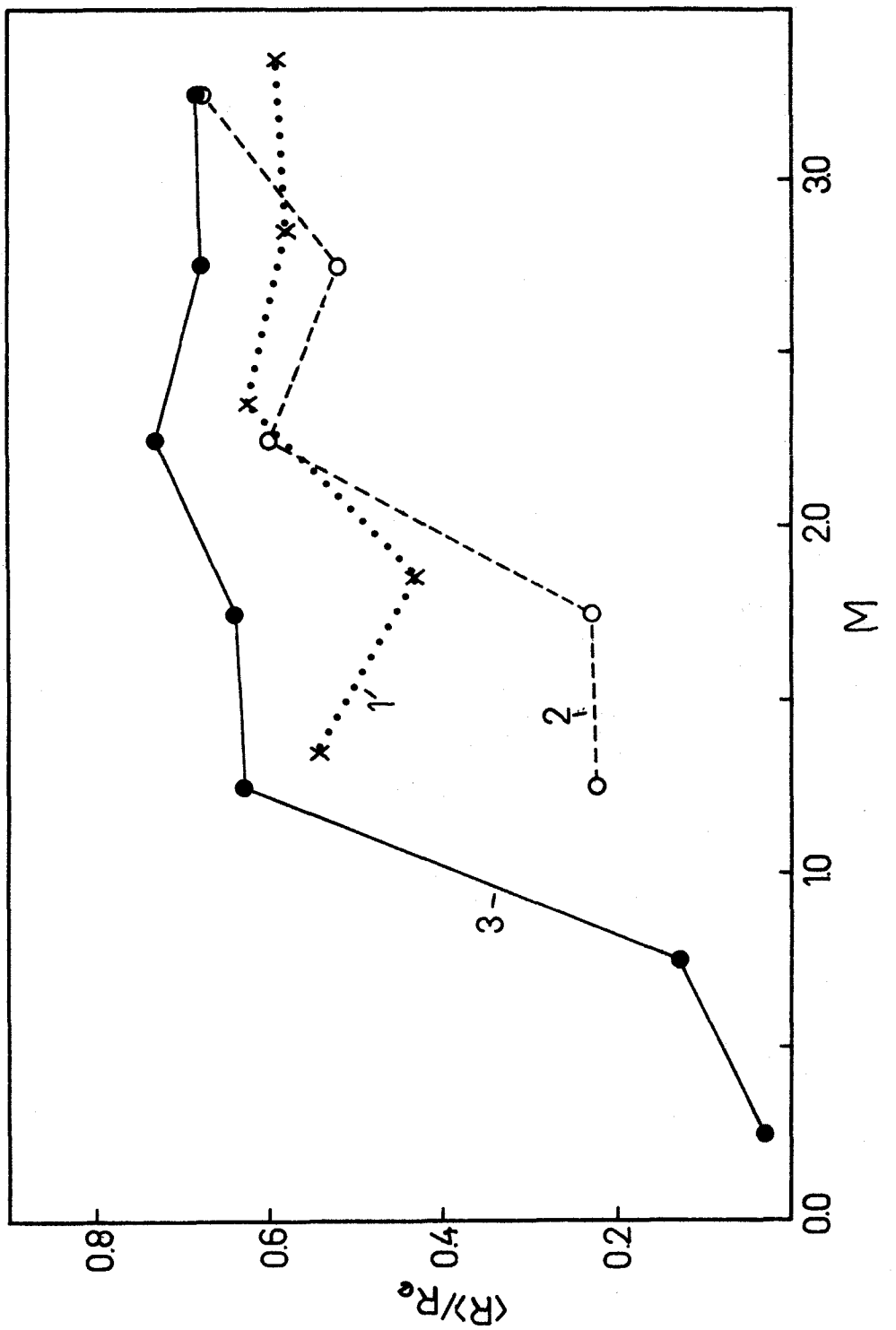

FIGURE 23.- The ratio of the mean radius of galaxies within R_G to that for a constant density distribution, as a function of magnitude. Curve 1 is for spiral rich clusters, curve 2 for spiral poor clusters and curve 3 for cD clusters.

VI. CONCLUSIONS

What can be concluded about the structure and evolution of clusters of galaxies from the information presented above? The most elementary fact is that, although we have neither searched for nor found the "missing mass", clusters must, indeed, be bound. The similarity in the virial theorem derived mass-luminosity ratios for most clusters, the agreement of profiles and mass segregation with theory, the similarity in features among clusters, the relations between size and luminosity and between compactness and galaxy content all make even more implausible than before the idea that clusters might not be bound.

If one follows the evolution of a bound system of particles, initially at rest, through its collapse and until it reaches a state of quasi-equilibrium, its qualitative behavior can be characterized by a constant increase in regularity and spherical symmetry, and by the growth of a dense core. With this in mind, it is tempting to regard the morphological sequence of spiral rich, spiral poor and cD clusters as a sequence in dynamical evolution.

The spiral rich clusters appear to be the youngest dynamically, and the evidence is quite strong that they are still in the process of collapse, as suggested originally by Gunn and Gott (1972). Their irregular mass distributions

could not survive the phase mixing and violent relaxation which occur during collapse. Their flat central density profiles are inconsistent with even the earliest Aarseth model, as is their lack of any mass segregation. Finally, the galaxy content of spiral rich clusters is very similar to that of the field, which is not true of the other cluster types. The relative compactness of one spiral rich cluster, A 1367, can be understood if we are seeing it at the moment of final collapse.

Conversely, it is equally certain that the spiral poor and cD clusters have collapsed and are approaching a steady state. They show all of the features expected from the models of collapsed clusters. Ignoring the feature at $0.5R_G$, the mass distributions in both core and envelope agree with the models, as does the mass segregation among the brighter galaxies. Their regularity and symmetry also distinguish them from the uncollapsed clusters.

It is quite possible that spiral rich clusters like the Hercules cluster will eventually become typical spiral poor clusters. One expects the necessary dynamical evolution to take place on collapse, and there only remains the problem of changing the galaxy content. The galaxy content of the two cluster types is such that the transmutation of some fraction of the spiral galaxies into S0's will change the spiral rich cluster content into that of a spiral poor

cluster. Gunn and Gott (1972) have shown how this might be done by the interaction of the gas content of a spiral galaxy with a hot intergalactic medium in the core of a cluster, and this theory provides the most natural explanation for the decrease in the density of spirals toward the center of spiral poor and cD clusters seen in Figures 27 and 28.

There is no equivalent mechanism for the transmuting of S0 into elliptical galaxies, and so the relation between spiral poor and cD clusters is not so clear. The direct collision of two stellar systems in which the dynamical time is comparable with the collision time tends to be inelastic (Aarseth and Hills, 1972, Toomre 1973), and thus the disks of two colliding S0 galaxies are likely to be sufficiently disrupted to make the final system elliptical in appearance. However, the frequency of direct collisions in a cluster is too low (Gunn and Gott 1972) and it is doubtful whether the tidal interaction in near encounters would be sufficiently strong.

Therefore, while the greater regularity and symmetry of the cD clusters, and their slightly steeper central profiles would suggest that they are dynamically older than the spiral poor clusters, their greater proportion of ellipticals seems to rule out the idea that they have evolved from the spiral poor clusters. These cluster types are, then, intrinsically different. If they are the dynamically oldest, and therefore

have evolved the fastest, the cD clusters must have begun as the densest fluctuations in the early universe. One could speculate, then, that their higher abundence of ellipticals is due to a birth rate of elliptical galaxies which increases with density relative to the other galaxy types.

All of the above discussion about cluster evolution rests on indirect arguments, but, if we know the mass to light ratios of particular clusters, the collapse times can be calculated directly.

We shall assume that a cluster of galaxies starts as a region of high density, which expands more slowly than the mean Hubble flow, finally coming to rest at a point of maximum expansion and then collapsing. If we assume that at the point of maximum expansion the cluster is a uniform density sphere, it is straightforward to show that its collapse time

$$t_c = \left(\frac{9\pi^2 \cdot M^2 \cdot G^2}{200 E_t^{\,3}} \right)^{1/2} \qquad (12)$$

where E_t is the total energy per unit mass. If the cluster, when observed now, is in virial equilibrium,

$$E_G = 2 \cdot E_t \qquad (13)$$

and, using equation 10,

$$t_c = 2.17 \times 10^{16} \frac{R_G^{\,3/2}}{L^{1/2}} \cdot \left(\frac{L}{M} \right)^{1/2} \text{years} \qquad (14)$$

where R_G is in megaparsecs and L in solar units.

Applying this equation to the five clusters with M/L of about 225, we find a mean t_c = 3.8 billion years. If we define

$$t^* = \frac{1}{t_c H_o} - 1 \qquad (15)$$

then, assuming q_o=0.0 and allowing one collapse time for the initial expansion of the cluster, t^* is the number of collapse times since the point of maximum expansion, i.e. it is the quantity t/t_c used in the models. Using H_o=50 km $s^{-1}Mpc^{-1}$ we find for this group of clusters t^* = 4.2 in agreement with our earlier deductions.

Applying these equations to A 2197 with M/L=54, we find t^* = 0.67, so this spiral rich cluster is still collapsing, as expected. But, even using the lower value of M/L=143, we find that for the spiral rich Hercules cluster t_c = 7.7 billion years and t^* = 1.61, indicating that it has collapsed. Using equations derived under the assumption of collapse, we obtain results consistent with collapse. Can a consistent solution be found with the Hercules cluster still collapsing?

Let us assume that t^* is slightly less than 1.0. From Figure 8, we see that, at this phase, $-E_G/E_k$= 1.5. In this case, the true value of M/L is 0.75 of the value calculated on the assumption of equilibrium, or 107±38. Also, $E_G = 3E_t$, so that, it is easily shown, the collapse time inferred from

the cluster's present gravitational energy is too short by a factor of 1.84. Since $t_c \sim \rho^{-1/2} \sim (M/L)^{-1/2}$, the collapse time calculated above is too short by a total factor of $1.84 \times (0.75)^{-1/2} = 2.12$, so, in fact, t_c = 16 billion years and $t^* = 0.23$, consistent with the assumption that the Hercules cluster is still collapsing.

We may, therefore, conclude that the high E:Sp ratio clusters are collapsed and have mass to light ratios of about 225, while low E:Sp ratio clusters are still collapsing and have mass to light ratios about one third of this value.

The only remaining mass-luminosity ratio , and the most difficult problem, is that of A 400. In appearance and galaxy content is is a spiral poor cluster, similar to A 194, but its mass to light ratio is the lowest of all, giving $t^* = 0.49$. Inspection of Figure 8 shows that at no time after collapse does $-E_G/E_K$ become sufficiently greater than 2.0 to appreciably increase M/L or t^*. Unless, then, the low mass-luminosity ratio is a statistical fluke or is due to measuring objects in some small subcluster or foreground group, A 400 is inconsistent with the picture of cluster evolution developed above.

The peculiar feature in the cluster profiles is the only other important and inexplicable phenomenon. If we believe the small bump in the spiral rich profile, this feature must be due to the initial distribution of mass in the cluster's

vicinity. It is true that any irregularity in the initial mass distribution will grow with time as the cluster collapses, but it is difficult to understand why all clusters should start with the same irregularity at almost the same radius. Also, it is suprising that the violent relaxation during collapse seems to amplify rather than smooth out this feature. Although this particular problem has not been studied, Aarseth and Hills (1972) have shown that irregularities in the form of subclustering are smoothed out during collapse. Clearly, more theoretical work needs to be done.

It would be nice to be able to compare the results of this study with theories of galaxy and cluster formation. Unfortunately, very few of these theories are able to make specific predictions about the present characteristics of galaxies and clusters. One of the few that does is that of Press and Schechter (1974) which, as pointed out earlier, correctly predicts the luminosity function of cluster members. It also predicts the constant density law for clusters found in Figure 15. Hopefully, other theories will also soon be developed to the point where they can be tested by the findings of this study.

REFERENCES

Aarseth, S.J., and Hills, J.G. 1972, Astr. and Ap., 21,255.

Abell, G.O. 1958, Ap. J. Suppl., 3, 211.

----------. 1962, in Problems of Extragalactic Research, ed. G.C. McVittie (New York: The Macmillan Co.)

Ables, H.D. and Ables, P.G. 1972, AAS Photo-Bulletin, no. 2.

Baade, W. and Spitzer, L. 1951, Ap. J., 113, 413.

Bahcall, N.A. 1971, A. J., 76, 995.

Burbidge, G.R. and Burbidge, E.M. 1959, Ap.J., 130, 629.

Chincarini, G. and Rood, H.J. 1972a, A.J., 77, 4.

----------. 1972b, A.J., 77, 448.

Clark, E.E. 1968, A.J., 73, 1011.

Fish, R.A. 1964, Ap.J., 139, 284.

Gunn, J.E. and Gott, J.R. 1972, Ap.J., 176, 1.

Kintner, E.C. 1971, A.J., 76, 409.

Matthews, T.A., Morgan, W.W. and Schmidt, M. 1964, Ap.J., 140, 35.

Minkowski, R. 1961, A.J., 66, 558.

Morgan, W.W. and Lesh, J.R. 1965, Ap.J., 142, 1364.

Noonan, T.W. 1973, A.J., 78, 26.

Oemler, A., Gunn, J.E. and Oke, J.B. 1972, Ap.J. (Letters), 176, L47.

Oemler, A. 1973, Ap.J., 180, 11.

Oke, J.B. and Schild, R.E. 1970, Ap.J., 161, 1015.

Peebles, P.J.E. 1970, A.J., 75. 13.

Press, W.H. and Schechter, P. 1974, Ap.J., in press.

Rood, H.J. and Baum, W.A. 1967, A.J., 72, 398.

----------. 1968, A.J., 73, 442.

Rood, H.J., Page, T.L., Kintner, E.C. and King, I.R. 1972, Ap.J., 175, 627.

Sandage, A. and Smith, L.L. 1963, Ap.J., 137, 1057.

Sandage, A. 1973, Ap.J., 183, 711.

Sargent, W.L.W. 1973, P.A.S.P., 85, 281.

Shectman, S.A. 1973, Ap.J., 179, 681.

----------. 1974, in preparation.

Toomre, A. 1973, I.A.U. Symposium no. 58.

Zwicky, F., Herzog, E., Wild, P., Karpowicz, M. and Kowal, C.T. 1961-1968, Catalogue of Galaxies and Clusters of Galaxies (Pasadena: Calif. Inst. of Tech.)

Zwicky, F. and Humason, M.L. 1964, Ap.J., 139, 269.